

# A variable star population in the open cluster NGC 6819 observed by the *Kepler* spacecraft

S. Sanjayan<sup>1,2</sup>, A.S. Baran<sup>1,3</sup>, P. Németh<sup>1,4,5</sup> and K. Kinemuchi<sup>6,7</sup>

<sup>1</sup>ARDASTELLA Research Group

<sup>2</sup>Centrum Astronomiczne im. Mikołaja Kopernika, Polskiej Akademii Nauk, ul. Bartycka 18, 00-716 Warszawa, Polska

<sup>3</sup>Astronomical Observatory, University of Warsaw, Al. Ujazdowskie 4, 00-478 Warszawa, Poland

<sup>4</sup>Astroserver.org, Fő tér 1, 8533 Malomsok, Hungary

<sup>5</sup>Astronomical Institute of the Czech Academy of Sciences, Fričova 298, CZ-251 65 Ondřejov, Czech Republic

<sup>6</sup>Department of Astronomy, New Mexico State University, Box 30001, MSC 4500, Las Cruces, NM 88003, USA

<sup>7</sup>Apache Point Observatory, 2001 Apache Point Road, P.O. Box 59, Sunspot, NM 88349-0059

November 22, 2022

## Abstract

We present the list of variable stars we found in the *Kepler* superstamp data covering approximately nine arcminutes from the central region of NGC 6819. This is a continuation of our work presented by Sanjayan *et al.* (2022a). We classified the variable stars based on the variability type and we established their cluster membership based on the available *Gaia* Data Release 3 astrometry. Our search revealed 385 variable stars but only 128 were found to be cluster members. In the case of eclipsing and contact binaries we calculated the mid-times of eclipses and derived ephemerides. We searched for eclipse timing variation using the observed minus calculated diagrams. Only five objects show significant orbital period variation. We used isochrones calculated within the MESA Isochrones and Stellar Tracks project and derived the average age (2.54 Gyr), average distance (2.3 kpc) and iron content  $[Fe/H] = -0.01(2)$ , of NGC 6819. We confirm this distance by the one derived from *Gaia* astrometry of the cluster members with membership probabilities greater than 0.9.

**Key words:** NGC 6819 - Open cluster - Kepler Mission - Variable stars

## 1. Introduction

In the notes of Caroline Herschel (Hoskin 2005), NGC 6819 was listed in the class of nebulae and star clusters found between  $\theta$  Lyra and  $\delta$  Cygni. Early study was mostly focused on photometry that allowed for construction of a color–

magnitude diagram (CMD) and to estimate the age of the cluster. Detecting only a weak nebula in photographic plates from the Palomar Observatory Sky Survey (POSS-I), King (1964) added NGC 6819 to the list of open clusters that may be old, which made the cluster exceptional as open clusters were considered to be young objects. The first photometry of 38 stars in the field of the cluster were done by Purgathofer (1966) who used the original plates from Barnard (1931). From a color-magnitude diagram Burkhead (1971) pointed out that the main sequence turnoff (MSTO) region of NGC 6819 is near to that of M67 hence both clusters have comparable ages, however no age of the latter was reported. Later Lindoff (1972) and Auner (1974) observed the cluster in the B-V color. They compared the MSTO and red giant branch (RGB) with other older clusters and predicted that the age of the cluster is at least 2.5 Gyr. From the theoretical isochrones Rosvick and Vandenberg (1998) reported an age of 2.4 Gyr, which is in agreement with the age 2.3(2) Gyr estimated by Anthony-Twarog *et al.* (2014). Rosvick and Vandenberg (1998) suggested that red clump (RC) stars are the descendants of blue stragglers (BS), given that NGC 6819 has a confirmed BS population. Kalirai *et al.* (2001) estimated a total mass of the cluster to be  $2\,600 M_{\odot}$ .

Many researchers undertook a search for a variable content in the area of the cluster. We compared our findings with the results reported in most of the following papers. Barkhatova and Vasilevsky (1967) conducted the first attempt to detect variable stars in NGC 6819 with a null result. A variable of the irregular type was reported for the first time by Lindoff (1971). As a result of search for contact binaries Kaluzny and Shara (1988) made the first significant discovery by detecting 11 variable stars but none of them were reported to be a contact binary. Manteiga *et al.* (1989) used RV data of stars in the area of the cluster and detected only one RV variable BS. Kryachko (2001) discovered two dwarf novae in the cluster area. A survey by Street *et al.* (2002) revealed 25 variable stars and 13 suspected variable stars in the area of NGC 6819. Street *et al.* (2003) did an extended search for planetary transits by analysing data of 38 000 stars in the area of NGC 6819, and they found 11 stars with transiting events. Street *et al.* (2005) reported a detection of 141 variable stars, including 53 eclipsing binaries, eight RS CVn variables, 70 rotational stars, 13 long period variables and five variables of other types. Stello *et al.* (2010) reported the first asteroseismic analysis of solar-like red giants in the cluster. Additional ground-based observations were taken by Talamantes *et al.* (2010) in the area of NGC 6819 and they listed 14 binaries and one  $\delta$  Scuti pulsator. Using the XMM-Newton data, Gosnell *et al.* (2012) made an unexpected discovery of 12 X-ray sources in the cluster area.

A time-series photometry of the cluster variable population allowed for an independent determination of a distance modulus and cluster age. Balona *et al.* (2013) used 129 rotational variables in NGC 6819 to study the relation between the period and B-V color, and they derived cluster age of about 2.5 Gyr. Basu *et al.* (2011) estimated the distance modulus of  $(m-M)_0 \approx 11.85$  mag and reddening  $E(B-V) \approx 0.15$  mag using asteroseismic analysis of red giant stars in the cluster. The authors estimated the distance to the cluster to be 2 344(24) pc. According to Salaris *et al.* (2004), NGC 6819 is located in the halo of the Milky Way and 300 pc above the galactic plane.

Spectroscopic observations allowed for determination of the motion in the Galaxy and the cluster metallicity. Using

only seven cluster members, Friel *et al.* (1989) derived the mean cluster radial velocity (RV) of  $-7(13)$  km/s. A more precise estimation of  $2.34(5)$  km/s was reported by Hole *et al.* (2009). Ak T *et al.* (2016) reported that the cluster has a slightly eccentric orbit with the eccentricity ( $e$ ) of 0.06 and has the orbital period of 142 Myr. According to Bragaglia *et al.* (2001), the cluster has a super solar metallicity of  $[Fe/H] = +0.09(3)$ , while Lee *et al.* (2015) pointed to a sub solar metallicity of  $[Fe/H] = -0.02(2)$ .

Stellar clusters are studied through their members, hence it is essential to identify cluster members. Below, we present a historical progress of a member hunt in NGC 6819. Sanders (1972) used the relative proper-motion of 189 stars in the cluster area and found 88 probable cluster members. Using RV measurements from the WIYN open cluster study XXIV, Hole *et al.* (2009) established membership of 913 stars in the cluster area, finding 437 targets to have probabilities greater than 50%. Stello *et al.* (2011) determined membership probability of 61 stars using asteroseismic analysis and found 50 members. Platais *et al.* (2013) derived 2 314 stars with more than 50% membership probability among 15 750 stars located in the cluster area. The authors used data from the WIYN open cluster study LV. Gao *et al.* (2015) established 537 cluster members by means of RVs and proper motion data. Zhang *et al.* (2015) presented membership studies of 80 stars using RVs from the Large Sky Area Multi-Object Fibre Spectroscopic Telescope (LAMOST) survey. Sampedro *et al.* (2017) determined the membership probability of 1 074 stars using the United States Naval Observatory (USNO) CCD Astrograph Catalog (UCAC4). The first membership analysis using *Gaia* astrometry was done by Cantat-Gaudin *et al.* (2018), who found 1 915 members. The cited works revealed many confirmed cluster members derived by means of RVs, proper motions, and seismic analysis. In Section 4 we present a comparison of the results of the membership studies reported by Cantat-Gaudin *et al.* (2018) with our results.

To increase the efficiency of the detection of all variable star populations in the cluster area, we undertook an analysis of all *Kepler* superstamp data of NGC 6819. The variable stars should in future serve the purpose of deriving the most precise parameters of the cluster, through binary star, asteroseismic and gyrochronology studies. In addition, *Gaia* data of the cluster members were used toward the cluster age and distance derivation. This is a continuation of our previous work on NGC 6791 presented by Sanjayan *et al.* (2022a). Recently, Colman *et al.* (2022) presented the light curves of KIC targets observed in the *Kepler* superstamps of NGC 6819 using an image subtraction technique. We stress that the method and analysis presented in this work is independent of the one presented in Colman *et al.* (2022).

In Section 2, we present a short description of the *Kepler* mission and data processing in order to obtain the light curves of variable stars. In Section 3, we present our analysis of spectra taken at Nordic Optical Telescope (NOT), Apache Point Observatory (APO) and other spectra we found in public databases i.e. LAMOST survey, Apache Point Observatory Galactic Evolution Experiment (APOGEE) survey, MMT Hectospec 300 optical fiber fed spectrograph survey, and Apache Point Observatory 3.5-meter telescope survey. In Section 4, we invoke the *Gaia* astrometric parameters of variable stars we detected to establish their cluster membership. In section 5, we report the zoo of variable stars we found in the area of NGC 6819. In Section 6, we present the results of the MIST (MESA Isochrones

and Stellar Tracks) isochrones fitting to estimate the age of and the distance to NGC 6819.

## 2. Kepler Photometry

During the original *Kepler* mission four open clusters (NGC 6791, NGC 6819, NGC 6811, NGC 6866) were continuously observed. NGC 6791 and NGC 6819 were observed in the so-called "superstamps", which were used for observing multiple targets in crowded fields. The central most parts NGC 6791 and NGC 6819 were covered during Quarters (Q) 1–17. In the first part of our work, we reported a detailed study of the *Kepler* superstamps of NGC 6791 (Sanjayan *et al.* 2022a).

We downloaded the *Kepler* superstamp data of NGC 6819 from the Mikulski Archive for Space Telescopes (MAST<sup>1</sup>). The data are 20 x 100 pixel boxes piled up in two contiguous 10 box stacks. The field of view of all pixels is 800 x 800 arcseconds and covers the central most part of the cluster. The superstamps data are collected in the long cadence mode, lasting 30 min. The pixel scale is 4 arcsec. The data were collected over 1460 days and are split into 18 quarters.

We searched for a flux variation by extracting fluxes for all time stamps in individual pixels for each of the quarters Q2–5. Next, a Fourier transform of the time-series data was performed in each pixel and each quarter separately. The pixels showing peaks (representing signal) in the amplitude spectra were selected. Signals that were identified with artifacts, either reported by Baran (2013) or those found in this project, were discarded. The optimal apertures are formed by contiguous pixels showing the same flux variation of  $S/N \geq 5$ , not including pixels that contain too much signal from neighbors, even though the  $S/N$  ratio is still  $\geq 5$ . Examples of optimal apertures can be seen in Figure 6 of Sanjayan *et al.* (2022b). To keep the solar cells facing sunlight, every quarter the spacecraft rolled 90 degrees, hence, with each quarterly rotation of the spacecraft, our targets landed on different CCD silicons. One CCD silicon covering the area of NGC 6819 had failed prior to Q6 data collection, which caused quarterly data gaps during Q6,10 and 14. Using the optimal apertures for all targets showing flux variation, we used PyKE software (Kinemuchi *et al.* 2012) to pull out the fluxes and correct them for instrumental artifacts by means of Co-trending Basis Vectors. Finally, using our custom scripts, we clipped the data at  $4.5\sigma$ , detrended using spline fits, and normalized them to *parts per thousand* (ppt). The variable stars detected in our work is presented in Section 5.

## 3. Spectroscopy

Using the Astrophysical Research Consortium's 3.5 m telescope at APO, we obtained spectra for 5 stars. The spectra were collected from the Dual Imaging Spectrograph (DIS), using the B1200 and R1200 grating. In the blue channel,

---

<sup>1</sup><https://archive.stsci.edu/>

the grating was centered at  $4\,300\text{ \AA}$  and had a wavelength range of  $1\,240\text{ \AA}$ , while for the red channel, the grating was centered at  $6\,400\text{ \AA}$  and had a range of  $1\,160\text{ \AA}$ . The linear dispersions are  $0.62\text{ \AA/pix}$  in the blue and  $0.58\text{ \AA/pix}$  in the red. The magnitude range of the stars were 14.08 to 18.70 in the Johnson V, and for one object, the *Gaia* G magnitude was 17.39. The spectra were reduced and extracted using standard IRAF single slit spectroscopic techniques (Tody 1986, 1993). We observed the spectra of eight pulsating variable stars with the 2.56 m NOT using ALFOSC spectrograph. In these spectra, we measured a dispersion of  $2.2\text{ \AA}$  from the full width at the half maximum of the lines in the arc spectra and a signal-to-noise ratio of  $\approx 100$  in the range of wavelengths  $4\,950\text{--}5\,300\text{ \AA}$ . For a number of targets we found spectra in the publicly available archives (links can be found in Table 1). HECTOSPEC (Fabricant *et al.* 2005) operates at a resolution of approximately  $R\approx 1\,000\text{--}2\,000$ , LAMOST (Zhao *et al.* 2012) offers low-resolution spectra with a resolution of around  $R\approx 1\,800$ , while APOGEE (Ahn *et al.* 2014, Majewski *et al.* 2017) covers the H-band ( $1.51\text{--}1.70\text{ }\mu\text{m}$ ) with a resolution of approximately  $R\approx 22\,500$ .

We followed the fitting procedures from Németh *et al.* (2012) in using XTGRID. The  $\chi$ -square minimizing steepest-descent procedure fits an observation with interpolated ATLAS 9 models, calculated in local thermodynamic equilibrium, drawn from the spectral library of Bohlin *et al.* (2017). Atmospheric parameters were derived by iteratively applying successive approximations of synthetic spectra to the observations. We interpolated in effective temperature ( $T_{\text{eff}}$ ), surface gravity ( $\log g$ ) and scaled solar metallicity ( $[M/H]$ ) space, and also fitted the radial velocity with respect to synthetic spectra. Iterations were pursued until the variation of surface parameters and the  $\chi$ -square decreased below 0.5%. Uncertainties of parameters were determined by changing  $[M/H]$  and radial velocities in one dimension until the statistical limit for 60% confidence was reached. The correlations between  $T_{\text{eff}}$  and  $\log g$  were considered by the procedure. To avoid local minima the fitting procedure returns to the global minimization if a better solution is found during these calculations. Further details of the analysis methods are presented in Section 3 of Sanjayan *et al.* (2022a). Fig. 1 shows the best-fit BOSZ/XTGRID model to the NOT/ALFOSC observation of KIC 5113357.

## 4. Cluster membership

Our goal was to use the *Gaia* Data Release 3 (DR3) astrometry to estimate the membership probability of all variable stars we found in this work. We downloaded astrometric data of over 36 000 stars from the *Gaia* DR3 catalogue (Gaia Collaboration *et al.* 2022). We selected the stars in the area of NGC 6819, defined by the cluster center  $\alpha_{2000} = 19:41:17.2$  and  $\delta_{2000} = +40:11:18$  (Kamann *et al.* 2019) and a tidal radius of 23 arcmin (Kalirai *et al.* 2001). The membership analysis was done using five astrometric parameters, position ( $\alpha$  and  $\delta$  in equatorial coordinates), proper-motion ( $\mu_\alpha$  and  $\mu_\delta$ ) and, parallax  $\pi$ . To establish the membership of our variable stars we followed the method used and described in Sanjayan *et al.* (2022a). It employs variational Bayesian inference model with Dirichlet process

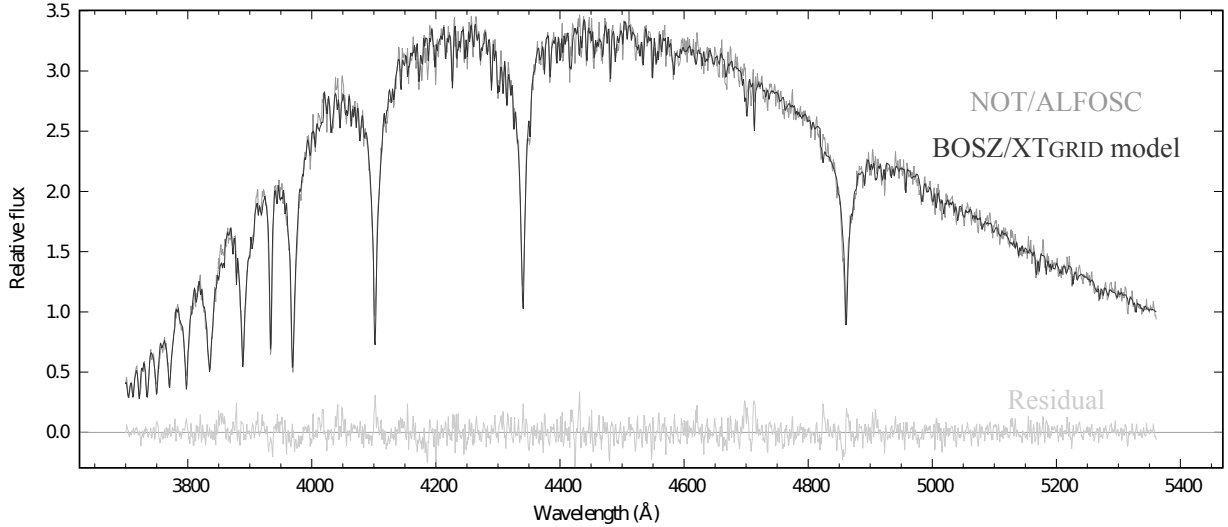


Figure 1: Best-fit BOSZ/XTGRID model to the NOT/ALFOSC observation of KIC 5113357.

prior (Ferguson 1973) using *scikit-learn* library in Python (Pedregosa *et al.* 2011). We found 1971 *Gaia* targets to be cluster members, including 128 variable stars. A CMD of 15 636 stars that were used in our analysis is presented in Fig. 2. Majority of stars we found to be members of NGC 6819 nicely mark the main sequence, red giant branch as well as BS and RC regions.

We compared 1527 stars identified as the cluster members with a membership probability at least 0.7, reported by Cantat-Gaudin *et al.* (2018), with members found in our analysis. We found 1482 stars to be cluster members. Of the remaining 45 stars, we found 19 to be outside our search radius, we excluded two stars due to high uncertainty in the parallax and proper motion, while we found 24 stars not to be members.

RV data in the *Gaia* DR3 allow us to enhance the membership analysis for some of the stars in our sample, however the data can be contaminated by binarity, rotation and pulsation effects. The data need to be free of these effects before applying to the membership analysis to obtain a reliable solution. We preliminarily assumed the *Gaia* DR3 RV data are clean of those effects and we used an RV as a sixth parameter in our analysis. We recalculated the membership probability of 821 stars for which we collected the RV data, deriving 126 cluster members. The membership of these 126 stars have not changed after using the RV data. This outcome validates either our assumption that RVs have no additional effects or any such effects do not affect the membership analysis. Using the RV data of these 126 cluster members we estimated the average radial velocity of the cluster to be +3.5(5) km/s.

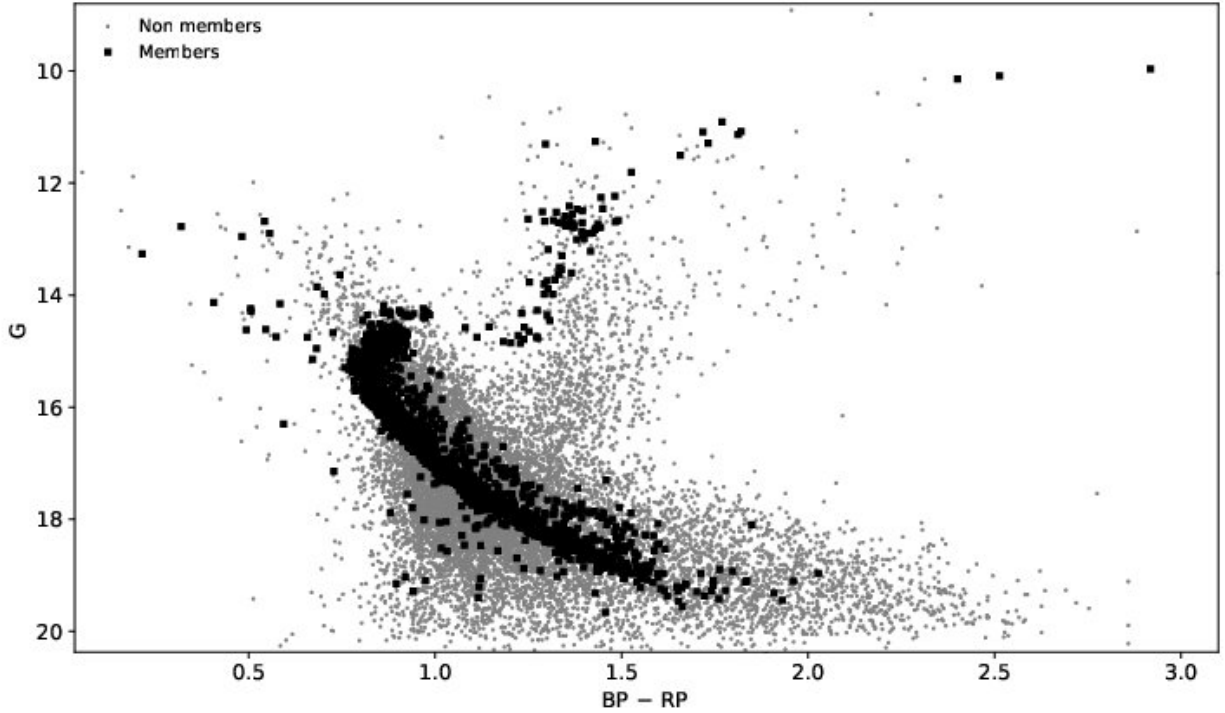


Figure 2: Color-magnitude diagram of all stars included in our analysis.

## 5. A zoo of variable stars

In total, we found 385 variable stars in the area of NGC 6819. The observed variability is classified based on the light curve shape and the periods estimated from an amplitude spectrum. We distinguished three main variability types, *i.e.*, binaries, pulsators and rotational. In addition, we listed several cases of unclassified and unidentified sources. Below we discuss each group of the flux variation. The cluster members and non members are listed in separate tables. For each type of variability we provide a number of newly detected variables.

We used amplitude spectra calculated from the light curves to classify pulsators into solar-like,  $\delta$  Scuti,  $\gamma$  Dor, and semi-regular variables. Stars with a periodic flux variation but showing additional flux modulation are classified as rotational stars. A sample of the light curves with corresponding amplitude spectra for each type of variability and specific classes we detected in this analysis is presented in Fig. 3.

We stress that our variability classification is subject to a number of caveats, which we have discussed in Sanjayan *et al.* (2022a) presenting similar work on NGC 6791. Therefore the location of targets, especially binaries, in the CMDs and our RV estimates should be considered with caution.

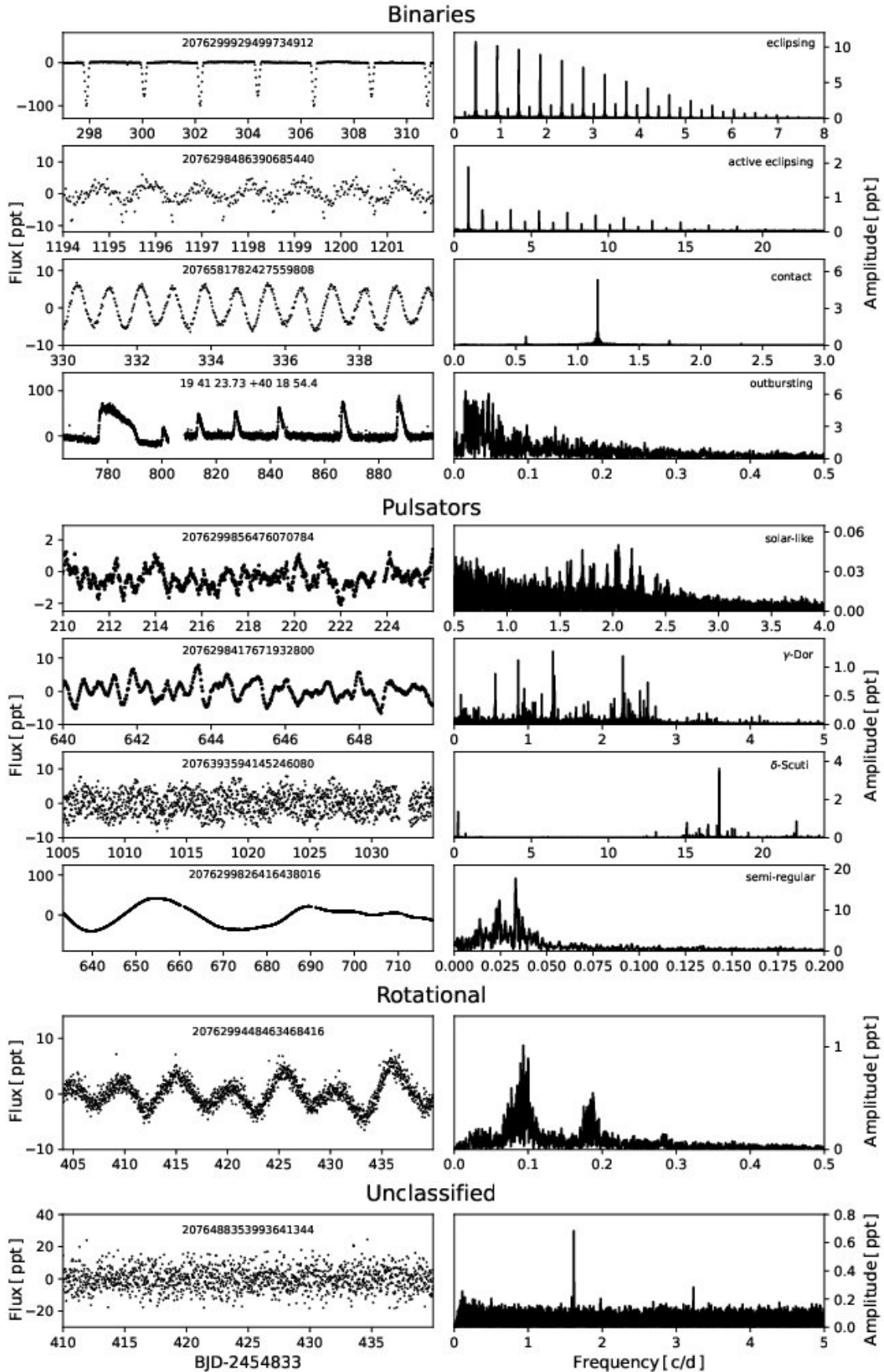


Figure 3: A sample of the light curves and amplitude spectra for different types and classes of variable stars in the area of NGC 6819.



## 5.1 Binary variables

We detected 59 binaries which included members, non members, and eight stars that are not associated with any *Gaia* targets, and hence their membership was not determined. From the phased light curves, we classified binaries into four classes, eclipsing, active eclipsing, contact and outbursting. We found 15 eclipsing systems with sharp eclipses and no out-of-eclipse variation. There are two members, 12 non-members, and one with no membership established. Eclipsing binaries with additional out-of-eclipse variation, likely caused by chromospheric activity, are called active eclipsing and we found eight members, 10 non-members and one with no membership established. The contact binaries are identified with systems showing light curves characteristics of W UMa system and we found seven members, 10 non-members and three with no membership established. Typical orbital periods of contact binaries are known not to be longer than 1 day so three stars may not be properly classified. Our classification is phenomenological, hence additional spectroscopic RV data may re-classify these objects. We found five outbursting stars, which we assumed to be binaries. Two of them are non-members while three have no membership established yet. In total we found 30 new variable binaries, including six cluster members, 17 field counterparts and seven with membership undetermined yet. We list the cluster members in Table 1, non-members in Table 5, while stars with no membership determined in Table 10. In Fig. 4 we present only phased light curves of the NGC 6819 member binaries that we found to be new discoveries. In a CMD shown in the top panel of Fig. 5, the majority of the binaries are located on the MS, while six are in the MSTO region. The latter ones can provide an independent estimate of the cluster age, if parameters are derived for individual components. As it was explained in Sanjayan *et al.* (2022a) the positions of binaries in the CMD should be treated with caution.

We identified five outbursting stars, which may possibly be associated with eruptions caused by a mass transfer. None of the outbursting stars were found to be members of the cluster. *Gaia* DR3 2076392906942365568 was reported as an X ray cataclysmic variable during the XMM Newton survey by Gosnell *et al.* (2012).

Using the eclipses in eclipsing systems and the light maxima in contact binaries, we estimated the midtimes by means of the method described in Kwee & van Woerden (1956). We used the midtimes to derive ephemerides, which are reported in Table 1 and 5. For a few cases we provided only rough estimates of periods, which is caused by a low precision of data. In two cases we detected single eclipses only. To search for an orbital period variation we calculated Observed minus Calculated (O-C) diagrams. We found significant orbital period variations in five binaries, including only one cluster member (Fig. 6). In two cases, KIC 5112759 and KIC 5113461, the variations may look sinusoidal caused by an additional body in these systems. The other three cases are not easy to interpret.

Table 1: List of binary stars that are cluster members. The newly discovered variables are marked in bold in the *Gaia* DR3 column. The data availability from MAST is denoted in the superscript of the KIC ID, where X means no data, L and S stands for the LC and SC data, respectively; the numbers before the letters represent how many quarters of data are available. CMD refers to the position in the color-magnitude diagram (MS - main sequence, MSTO - main sequence turn off, RGB - red giant branch, BS - blue straggler, AGB - asymptotic giant branch, RC - red clump, HB - horizontal branch, EHB - extreme horizontal branch). The superscript <sup>e</sup> of the period denotes significantly eccentric orbit. The superscript <sup>+</sup> of the CMD indicates that not all five astrometric parameters were used in the membership analysis. HRD refers to a position in the  $T_{\text{eff}}$ ,  $\log g$  diagram. The source of the spectra is marked in the Ref column, i.e. 1 - HECTOSPEC, 2 - NOT, 3 - LAMOST, 4 - APO35, and 5 - APOGEE. The \* indicates that the atmospheric parameters are derived in this work.

<i>Gaia</i> DR3	KIC	$P_{\text{orb}}$ [days]	$T_0$ [BJD]	G [mag]	CMD	HRD	$T_{\text{eff}}$ [K]	logg	RV [km/s]	[Fe/H]	Ref
<b>2076300062631198208</b>	5024475 <sup>X</sup>	0.35461351(48)	2 454 964.3935(11)	16.950	MS	-	-	-	-	-	-
2076298864347818624	5024447 <sup>14L</sup>	771.8122(14)	2 455 267.6048(10)	14.933	MS	-	-	-	-	-	-
2076300101298442368	5112456 <sup>X</sup>	1.04163866(35)	2 454 965.06811(26)	16.943	MS	MS	5 660(200)	4.36(1)	0(13)	-0.439(31)	4 *
2076299929499734912	5024292 <sup>1S,4L</sup>	4.3010306(16)	2 454 967.449238(30)	15.001	MS	-	-	-	-	-	-
2076299826420588288	5024450 <sup>1S,11L</sup>	3.0518491(12)	2 455 185.42743(27)	14.985	MS	-	-	-	-	-	-
2076487121349914752	5023948 <sup>1S,9L</sup>	3.64930727(38)	2 455 465.83818(6)	14.991	MS	-	-	-	-	-	-
2076299169277916160	5024064 <sup>X</sup>	2.05541020(25)	2 454 965.97867(10)	18.528	MS	-	-	-	-	-	-
<b>2076298486390685440</b>	5024364 <sup>X</sup>	1.089253(5)	2 454 965.8187(39)	16.982	MS	-	-	-	-	-	-
2076393422338668800	5113176 <sup>X</sup>	2.50489870(38)	2 454 964.84980(12)	18.973	MS	-	-	-	-	-	-
<b>2076392838230907264</b>	5024980 <sup>X</sup>	414.54921(33) <sup>e</sup>	2 455 081.23049(61)	17.427	MS	-	-	-	-	-	-
2076581713708050176	5112407 <sup>X</sup>	0.366025967(25)	2 454 964.90170(5)	16.415	MS	MS	5 620(50)	4.345(37)	65(3)	-1.15(8)	1 *
2076299792060826496	5024624 <sup>X</sup>	0.30321101(8)	2 454 964.70244(22)	17.097	MS	MS	5 590(20)	4.865(23)	26(2)	-0.430(23)	1 *
2076299448463338368	5023989 <sup>X</sup>	0.26367746(8)	2 454 964.78122(23)	19.508	- <sup>+</sup>	-	-	-	-	-	-
<b>2076581782427559808</b>	5112708 <sup>X</sup>	1.7195289(19)	2 454 965.2048(9)	14.915	MS	-	-	-	-	-	-
2076394105234042496	5112759 <sup>X</sup>	0.25622643(8)	2 454 964.66578(25)	17.788	MS	MS	4 650(30)	4.184(28)	15(5)	-0.67(7)	1 *
<b>2076389608415499392</b>	5025105 <sup>X</sup>	1.5747014(35)	2 454 965.1646(19)	15.286	MS	-	-	-	-	-	-
<b>2076300066938740096</b>	5112693 <sup>X</sup>	0.211752(1)	2 454 964.59610(38)	16.828	MS	-	-	-	-	-	-

HECTOSPEC - <https://oira.cfa.harvard.edu>, APOGEE - <https://www.sdss.org/dr/16/irspec>, LAMOST - <http://dr6.lamost.org>, APO 35 - <https://www.apo.nmsu.edu>

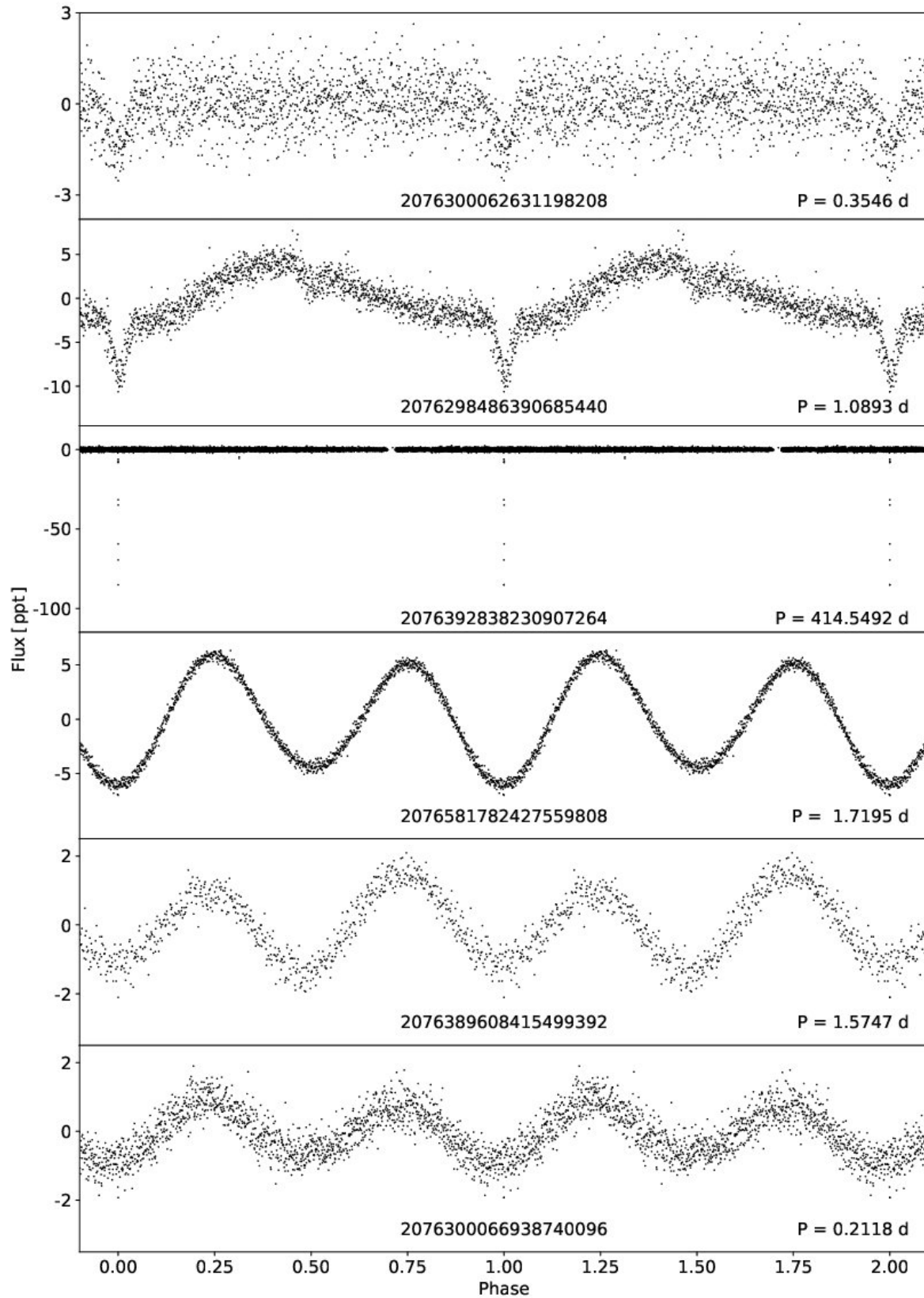


Figure 4: Phased light curves of newly found cluster member binaries. See Table 1 for details.

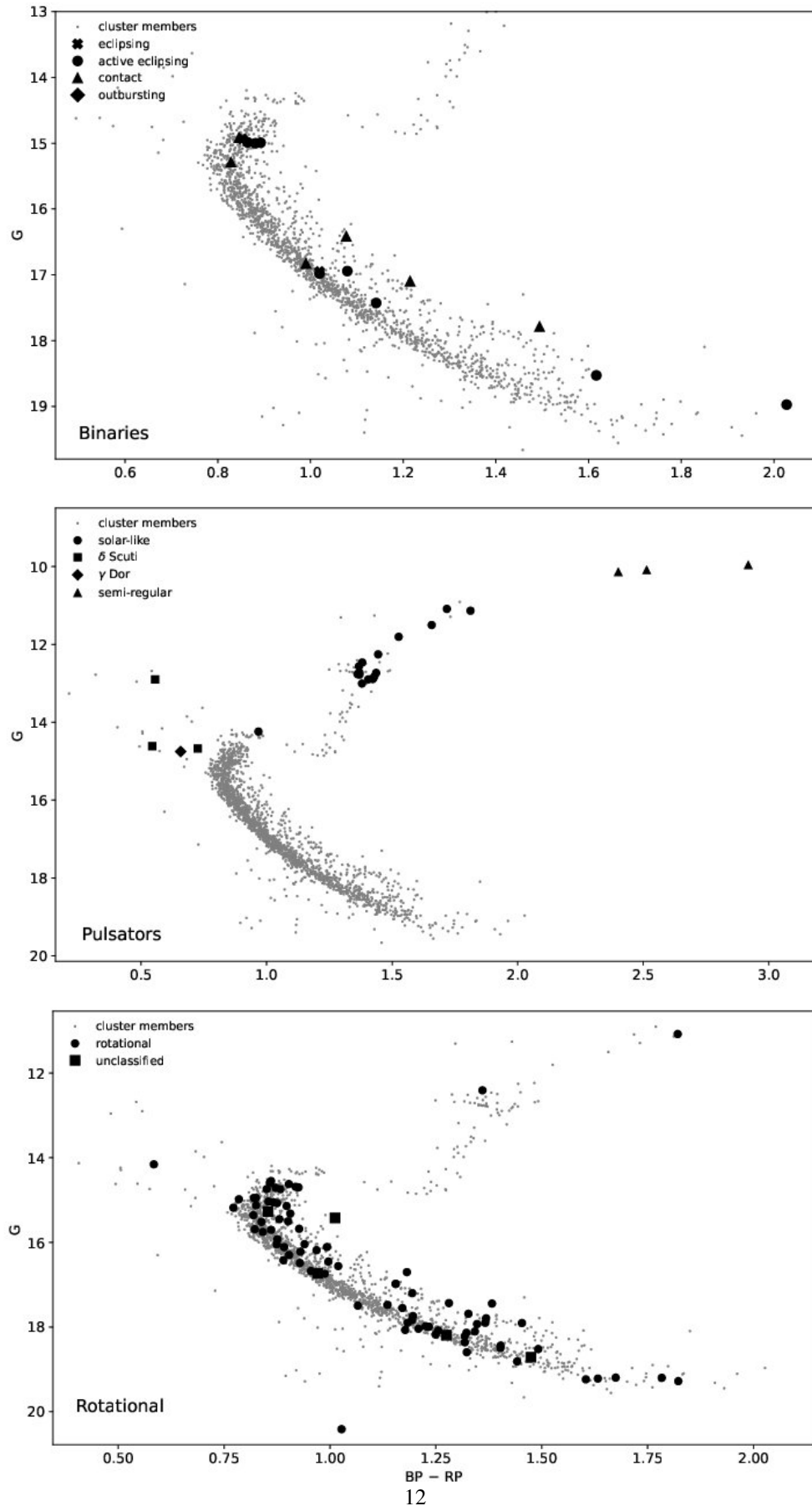


Figure 5: Color-magnitude diagram of NGC 6819. Binaries, pulsators, and rotational/unclassified cluster members are marked in the top, middle, and bottom panels, respectively.

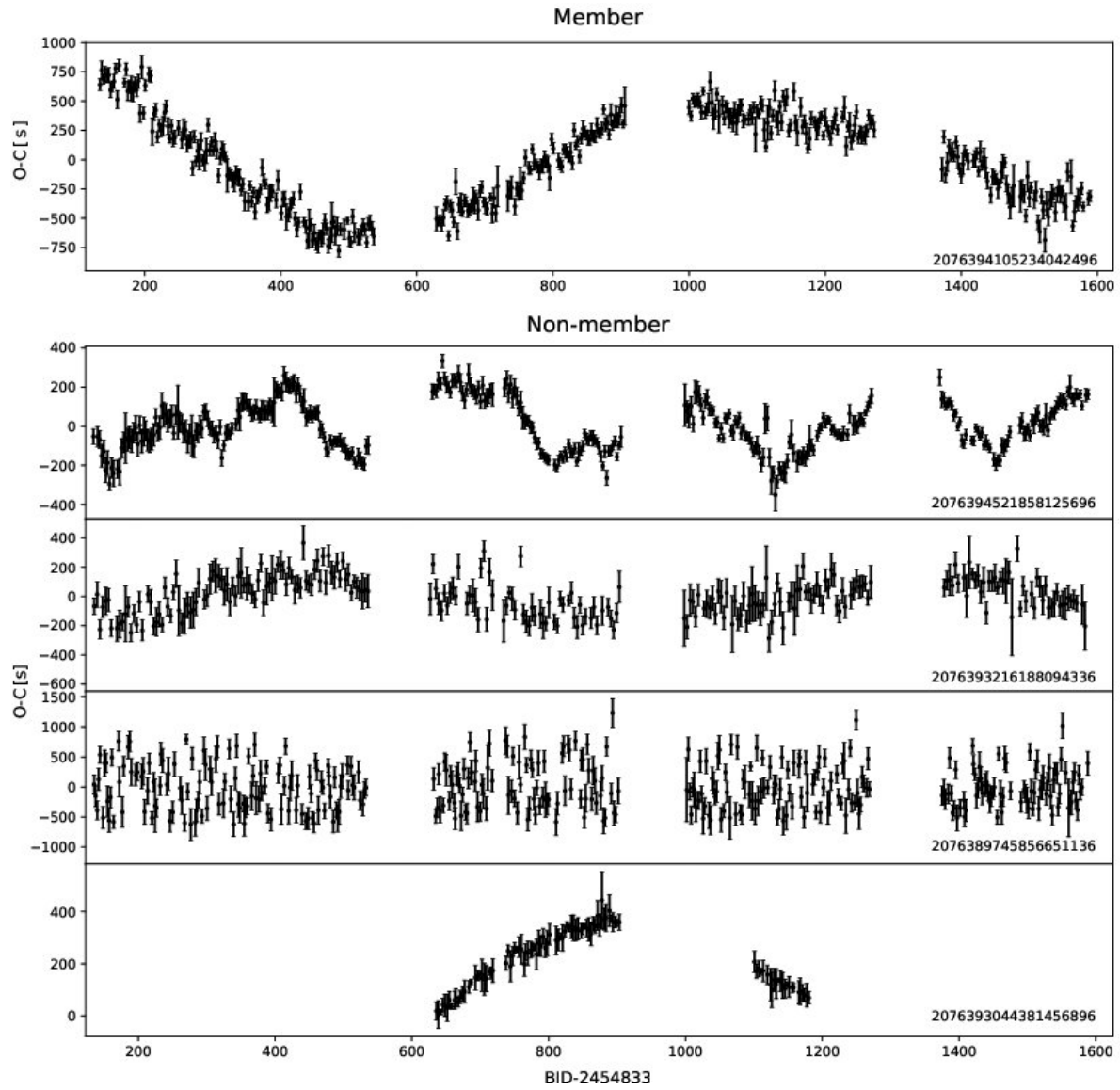


Figure 6: O-C diagrams of four contact and one active eclipsing systems showing significant orbital period variations. *Gaia* DR3 numbers are given in the bottom right corners.

## 5.2 Pulsators

We found a flux variation in 69 stars, which we interpreted as stellar oscillations and we separated the following classes, solar-like,  $\delta$  Scuti,  $\gamma$  Doradus and semi-regular pulsators. We found 24 pulsating cluster members including 17 solar-like, three  $\delta$  Scuti, one  $\gamma$  Doradus and three semi-regular. The field counterpart includes, 34 solar-like, two  $\delta$  Scuti, six  $\gamma$  Doradus and three semi-regular pulsators. In total we found 32 new variable pulsators, including two cluster members and 30 field counterparts. We present the pulsating cluster members in Table 2 and the field counterpart in Table 6. The location of the former group in the CMD is shown in the middle panel of Fig. 5. A detailed analysis of solar-like and  $\delta$  Scuti/ $\gamma$  Doradus pulsators will be reported by Themessl *et al.* (in prep.) and Guzik *et al.* (2023), respectively.

The majority of pulsating cluster members are located on the RGB, six are the RC objects, while four  $\delta$  Scuti and  $\gamma$  Doradus objects seems to be located in the BS region. The semi-regular pulsators are the asymptotic giant branch (AGB) objects.

Since this work is also a part of our search for pulsating extreme horizontal branch stars, we specifically looked for any flux variation that is characteristic of pulsating hot subdwarfs identified in NGC 6791 and reported by Sanjayan *et al.* (2022a) and (2022b). Hot subdwarfs can be formed through either a degenerate or a non-degenerate channel. The former channel works only for progenitor masses up to around 2.2 solar masses. Such stars need significantly less time than 2.5 Gyr to settle down onto the HB and even to reach the end of the white dwarf (WD) cooling tracks, becoming too faint to be detected. The latter channel is available for progenitors more massive than around 2.2 solar masses. Given the age of the cluster, stars with masses in a range of 1.5 – 1.6 solar masses had enough time to evolve to the HB and, if most of the hydrogen is lost, to become hot subdwarfs. More massive stars could have evolved to become post-HB stars (the most massive ones can now be very cool WDs and too faint to be seen), while less massive stars are still on the RGB or the MS, if less massive than 1.45 solar masses. Our consideration leads to a conclusion that the CMD of NGC 6819 should be well populated with stars all the way from the MS to the WD stage. This is not what we can see in Fig. 5. There is neither the WD nor the extreme HB populations. We stress that our consideration is based on a single star evolutionary time scale. Binary channels contributing either to a mass loss or a merger event can extend the time scale significantly, which could explain a lack of the hot subdwarf population in this cluster.

## 5.3 Rotational Variables

Stars showing modulated periodic flux variations are classified as rotational variables. Such a flux modulation can also be verified by amplitude spectra showing complex peak profile, as a consequence of amplitude/frequency variation. The rotational variability is usually identified with migrating star spots on the stellar surface. Our classification of rotational variables may not always be correct, since it can be mimicked *e.g.* by small amplitude ellipsoidal variability

Table 2: List of cluster members showing pulsations. See caption of Table 1 for explanation.

<i>Gaia</i> DR3	KIC	G [mag]	CMD	HRD	T <sub>eff</sub> [K]	logg	RV [km/s]	[Fe/H]	Ref
solar-like									
2076488427020005632	5111940 <sup>14L</sup>	13.005	RGB	RGB	4 771(92)	2.79(11)	2.964(71)	0.200(28)	5
2076581919866484224	5112401 <sup>15L</sup>	12.562	RC	RC	4 842(92)	2.65(11)	2.488(60)	0.200(27)	5
2076487872957025408	5112387 <sup>15L</sup>	12.776	RC	RC	4 839(92)	2.85(11)	2.80(22)	0.200(28)	5
2076581713708596352	5112481 <sup>15L</sup>	14.239	RGB	RGB	4 152(69)	1.66(8)	-1.664(80)	0.000(25)	5
2076487838597288320	5112373 <sup>15L</sup>	12.755	RC	RC	4 821(92)	2.73(11)	2.29(51)	0.200(28)	5
2076300101298433792	5024297 <sup>14L</sup>	12.896	RGB	–	–	–	–	–	–
2076299792060819328	5024583 <sup>14L</sup>	12.732	RGB	RGB	4 687(92)	2.55(11)	1.9843(34)	0.200(27)	5
<b>2076299856476070784</b>	5024511 <sup>X</sup>	12.256	RGB	–	–	–	–	–	–
2076394659297111552	5113061 <sup>15L</sup>	11.088	RGB	RGB	4 221(92)	1.67(11)	2.56(11)	0.100(26)	5
2076581816787312896	5112744 <sup>15L</sup>	12.890	RGB	RGB	4 691(92)	2.63(11)	2.7996(89)	0.100(28)	5
2076393937742523904	5112730 <sup>15L</sup>	12.719	RC	RC	4 823(92)	2.72(11)	1.350(75)	0.200(27)	5
2076393692914035456	5112786 <sup>15L</sup>	11.502	RGB	RGB	4 308(92)	1.86(11)	3.824(45)	0.100(27)	5
2076393869023076608	5112948 <sup>14L</sup>	12.833	RGB	RGB	4 766(92)	2.68(11)	3.588(24)	0.200(27)	5
2076393765943846656	5112938 <sup>14L</sup>	12.762	RC	RC	4 842(92)	2.69(11)	1.328(28)	0.200(27)	5
2076393624194561152	5024750 <sup>15L</sup>	11.806	RGB	RGB	4 501(92)	2.11(11)	2.177(27)	0.100(27)	5
2076299860780325504	5024601 <sup>14L</sup>	12.465	RC	–	–	–	–	–	–
2076298761268676352	5024851 <sup>15L</sup>	11.136	RGB	RGB	4 159(92)	1.60(11)	6.23(23)	0.100(26)	5
$\delta$ -Scuti									
2076299826420542080	5024468 <sup>X</sup>	12.898	BS	BS	7 770(50)	4.38(10)	-14(2)	-0.2(1)	2*
2076299482823088000	5024084 <sup>1S,14L</sup>	14.674	BS	–	–	–	–	–	–
<b>2076393594145246080</b>	5113357 <sup>X</sup>	14.613	BS	BS	7 270(50)	3.70(5)	65(3)	-0.53(10)	2*
$\gamma$ -Dor									
2076298417671932800	5024455 <sup>1S,14L</sup>	14.751	BS	–	–	–	–	–	–
semi-regular									
2076299826416438016	5024470 <sup>X</sup>	9.964	AGB	–	–	–	–	–	–
2076582950658667264	5199859 <sup>15L</sup>	10.143	AGB	AGB	3 828(92)	1.00(11)	2.1875	-0.200(27)	5
2076394728016615680	5113517 <sup>1L</sup>	10.091	AGB	–	–	–	–	–	–

or unstable long-period pulsations. Light curves showing stable periodic flux variations are classified as binaries, since we do not expect non migrating star spots.

In total, we found 233 variable stars showing rotational variability, which makes them the most abundant variable population in NGC 6819. There are 82 cluster members (Table 3), 136 field counterparts (Tables 7 and 8), and 15 stars with no membership established (Table 10). The periods of rotational variables are in a wide range of 0.2–45 days. Cross matching our list of rotational variables with the International Variable Star Index (VSX) catalogue, we found 15 rotational variables to be of BY Draconis type, while KIC 5112508 is a rotating X ray binary reported by Gosnell *et al.* (2012). In summary, we found 185 new variable rotating stars, including 70 cluster members, 100 field counterparts and 15 with membership undetermined yet. The location of the cluster members in the CMD is shown in the bottom panel of Fig. 5.

#### 5.4 Unclassified and unidentified variables

In the case of 24 stars, we were unable to classify their variability types. The data are either not precise or it is not too clear if the shape of a light curve remains stable over time. The latter argument is essential to distinguish between binaries and rotational variables. An example of a light curve in an unclassified group is presented in the bottom panel of Fig. 3. We identified five variables to be cluster members, 18 non-members and one with membership undetermined, and they are listed in Table 4, 9 and 10, respectively. All field stars, four members and the one with no membership, are new variables detected in this work. The newly discovered variable KIC 5023913 exhibits low frequency pulsations, similar to solar-like ones, and is positioned near the MS on the CMD. However, it cannot be classified as a solar-like pulsator due to the limited sampling of the *Kepler* long cadence data, which is insufficient to detect MS pulsation occurring beyond the Nyquist limit. KIC 5112843 shows two close frequencies with high amplitudes, which translates into beating in a light curve. The star may be a binary system, as discussed by Guzik *et al.* (2023), however it does not fit into any of our four binary classes. We leave such cases for future investigation. The location of the cluster members in the CMD is shown in the bottom panel of Fig. 5.

We found signals in amplitude spectra, associated with optical counterparts in the Pan-STARRS (Chambers *et al.* 2016, Flewelling *et al.* 2020) survey that do not have *Gaia* designations. Only one star has a custom designation and was reported in the past. The remainder of the stars are given by coordinates. We classified the signal to a proper variability type and estimated its period. These stars were included in the counts of the variability types discussed in the previous subsections. We show the list of these unidentified objects in Table 10. Since the stars are not listed in the *Gaia* catalog, we are unable to estimate their membership.



Table 3: List of cluster members showing rotational variability. See caption of Table 1 for explanation.

<i>Gaia</i> DR3	KIC	Period [days]	G [mag]	CMD	HRD	$T_{\text{eff}}$ [K]	logg	RV [km/s]	[Fe/H]	Ref
2076489148574565888	5112059 <sup>X</sup>	22.3010	17.901	MS	—	—	—	—	—	—
2076489217294036352	5199551 <sup>X</sup>	23.1662	17.495	MS	—	—	—	—	—	—
2076488942416130688	5112104 <sup>30S,11L</sup>	5.6490	14.593	MSTO	—	—	—	—	—	—
2076488869389772800	5112151 <sup>X</sup>	18.5003	18.812	MS	—	—	—	—	—	—
2076492034792541952	5111815 <sup>14S</sup>	3.5750	14.948	MS	—	—	—	—	—	—
2076488495739451136	5111800 <sup>X</sup>	3.8679	15.181	MS	—	—	—	—	—	—
2076488770617529088	5112068 <sup>X</sup>	15.9215	14.982	MS	—	—	—	—	—	—
2076488152142173312	5112298 <sup>X</sup>	2.3639	15.688	MS	—	—	—	—	—	—
2076488319633886336	5111907 <sup>X</sup>	15.7120	18.175	MS	—	—	—	—	—	—
2076488289581014400	5111849 <sup>1S,2L</sup>	5.9651	14.551	MSTO	—	—	—	—	—	—
2076488147835261696	5112257 <sup>X</sup>	19.5174	18.594	MS	—	—	—	—	—	—
2076488903749503104	5112187 <sup>X</sup>	19.6927	19.217	MS <sup>+</sup>	—	—	—	—	—	—
2076487945983692672	5112173 <sup>X</sup>	7.1660	16.702	MS	—	—	—	—	—	—
2076487568026522880	5111983 <sup>X</sup>	6.1842	17.794	MS	—	—	—	—	—	—
2076300135658207232	5112512 <sup>X</sup>	5.5446	16.422	MS	—	—	—	—	—	—
2076300131350662912	5112490 <sup>X</sup>	7.5360	16.452	MS	—	—	—	—	—	—
2076393972102236800	5112566 <sup>X</sup>	11.0660	17.832	MS	—	—	—	—	—	—
2076487808537778688	—	0.9752	19.236	MS	—	—	—	—	—	—
2076300101298445184	5112431 <sup>X</sup>	5.2943	16.739	MS	—	—	—	—	—	—
2076300066938738176	5112630 <sup>X</sup>	4.4602	15.141	MS	—	—	—	—	—	—
2076300131353981312	5112536 <sup>X</sup>	0.6732	17.686	MS	—	—	—	—	—	—
2076300101298455168	5112519 <sup>X</sup>	5.9061	17.900	MS	—	—	—	—	—	—
2076300101299126912	5112434 <sup>X</sup>	5.0307	14.740	MSTO	—	—	—	—	—	—
2076393903382760576	5112677 <sup>X</sup>	7.1078	14.707	MSTO	—	—	—	—	—	—
2076299826420536320	5024456 <sup>14L</sup>	3.2313	11.079	RGB	RGB	4 062(69)	1.49(8)	1.383(76)	0.000(25)	5
2076487082683547008	5023857 <sup>X</sup>	11.5019	18.360	MS <sup>+</sup>	—	—	—	—	—	—
2076300066938722176	5024480 <sup>X</sup>	4.1951	15.679	MS	—	—	—	—	—	—
2076299585902316416	5024114 <sup>X</sup>	11.9194	15.754	MS	—	—	—	—	—	—
2076299723341297920	5024318 <sup>X</sup>	3.7930	15.516	MS	—	—	—	—	—	—
2076299929499804288	5024287 <sup>1S,1L</sup>	7.1699	14.623	MS	—	—	—	—	—	—
2076299963859447936	5024151 <sup>X</sup>	45.9273	14.157	BS	—	—	—	—	—	—
2076299448463468416	5023967 <sup>X</sup>	10.6964	16.676	MS	—	—	—	—	—	—
2076299757701068800	5024600 <sup>X</sup>	3.9612	16.221	MS	—	—	—	—	—	—
2076299723341302272	5024403 <sup>X</sup>	5.0020	15.704	MS	—	—	—	—	—	—
2076299036142588032	5024760 <sup>X</sup>	2.4474	16.043	MS	—	—	—	—	—	—
2076299753393405312	5024526 <sup>X</sup>	8.0142	18.520	MS	—	—	—	—	—	—
2076299688981553280	5024365 <sup>1S,1L</sup>	7.4463	14.700	MSTO	—	—	—	—	—	—
2076299001786815104	5024641 <sup>14L</sup>	5.6497	14.742	MSTO	—	—	—	—	—	—
2076298963119414912	5024756 <sup>X</sup>	21.7471	17.979	MS	—	—	—	—	—	—
2076298417671212800	5024491 <sup>X</sup>	4.0566	16.486	MS	—	—	—	—	—	—
2076298310287835776	4936866 <sup>X</sup>	20.9493	17.739	—	—	—	—	—	—	—
2076582465319137792	5200072 <sup>X</sup>	10.0885	18.497	MS	—	—	—	—	—	—
2076581851136420608	—	0.2074	20.413	MS <sup>+</sup>	—	—	—	—	—	—
2076396171125625984	5200422 <sup>14L</sup>	5.1932	14.950	MS	—	—	—	—	—	—
2076581675044794112	5112589 <sup>X</sup>	7.3381	17.476	MS	—	—	—	—	—	—
2076394075181506688	5112866 <sup>X</sup>	0.4869	17.434	MS	—	—	—	—	—	—
2076394006454008320	5112675 <sup>X</sup>	4.3123	16.720	MS	—	—	—	—	—	—
2076394006461998336	5112698 <sup>X</sup>	3.6742	15.321	MS	—	—	—	—	—	—
2076393903382776576	5112699 <sup>X</sup>	2.3101	15.925	MS	—	—	—	—	—	—
2076393869023084288	5112979 <sup>11L</sup>	23.2479	15.034	MS	—	—	—	—	—	—
2076394002154821632	5112736 <sup>X</sup>	21.9286	18.039	MS	—	—	—	—	—	—
2076393933435330688	5112777 <sup>X</sup>	5.9733	17.445	MS	—	—	—	—	—	—
2076393899075931904	5112682 <sup>X</sup>	8.7219	19.198	MS <sup>+</sup>	—	—	—	—	—	—
2076393800303612032	5113045 <sup>X</sup>	22.2631	15.054	MS	—	—	—	—	—	—
2076393903382776704	5112710 <sup>X</sup>	19.6045	15.451	MS	—	—	—	—	—	—
2076393697224343296	5112781 <sup>X</sup>	2.6031	18.105	MS	—	—	—	—	—	—
2076393869023085440	5113010 <sup>X</sup>	1.4268	15.357	MS	—	—	—	—	—	—
2076394178252904320	5113076 <sup>X</sup>	13.3217	18.439	MS	—	—	—	—	—	—
2076393319267340288	5113478 <sup>X</sup>	0.8781	16.560	MS	—	—	—	—	—	—
2076393662865120256	5112908 <sup>X</sup>	4.7402	16.980	MS	MS	5 500(30)	4.47(7)	18(2)	-0.43(9)	1 *
2076393731584598528	5112852 <sup>X</sup>	4.5927	16.185	MS	—	—	—	—	—	—
2076393628504856448	5024697 <sup>X</sup>	3.3347	16.109	MS	—	—	—	—	—	—
2076393692914036608	5112741 <sup>14L</sup>	17.6960	12.408	RC	RC	4 814(107)	2.64(17)	-38(5)	-0.08(10)	3
2076393044389353984	5113099 <sup>X</sup>	23.3089	17.201	MS	—	—	—	—	—	—
2076393765944335104	5113001 <sup>14L</sup>	6.5676	14.687	MSTO	—	—	—	—	—	—
2076393662865120256	5112908 <sup>X</sup>	2.9060	16.980	MS	—	—	—	—	—	—
2076393284907576960	5113426 <sup>X</sup>	7.3628	18.081	MS	—	—	—	—	—	—
2076393147460788864	5113295 <sup>11L</sup>	28.6162	16.112	MS	RGB	5 420(400)	3.5(5)	-34(6)	1.5(5)	1 *
2076392838230907392	5024988 <sup>X</sup>	5.4480	15.502	MS	—	—	—	—	—	—
2076392868287903872	5024774 <sup>X</sup>	2.8742	17.551	MS	—	—	—	—	—	—
2076392872590614784	5024751 <sup>X</sup>	3.4953	17.904	MS	—	—	—	—	—	—
2076390295610350464	5113519 <sup>X</sup>	10.9769	17.991	MS	—	—	—	—	—	—
2076392730841568640	5025077 <sup>X</sup>	21.7111	17.929	MS	—	—	—	—	—	—
2076392975669885568	5113165 <sup>X</sup>	6.4769	16.297	MS	—	—	—	—	—	—
2076392799560963584	—	20.2391	19.278	MS <sup>+</sup>	—	—	—	—	—	—
2076389711494716800	5025150 <sup>X</sup>	6.3577	15.074	MS	—	—	—	—	—	—
2076389878983223808	5025470 <sup>X</sup>	22.1879	18.216	MS	—	—	—	—	—	—
2076300066938729856	5112574 <sup>X</sup>	1.6160	16.045	MS	—	—	—	—	—	—
2076393800295734144	5113026 <sup>X</sup>	20.8330	18.069	MS	—	—	—	—	—	—
2076298967427112448	5024801 <sup>X</sup>	1.8472	15.123	MS	—	—	—	—	—	—
2076488049055863936	—	6.8456	19.194	MS	—	—	—	—	—	—
2076299856472624128	—	17.8793	18.135	MS	—	—	—	—	—	—

Table 4: List of cluster members with unclassified variability. See caption of Table 1 for explanation.

<i>Gaia</i> DR3	KIC	Period [days]	G [mag]	CMD	HRD	$T_{\text{eff}}$ [K]	logg	RV [km/s]	[Fe/H]	Ref
<b>2076488353993641344</b>	5111986 <sup>X</sup>	0.6185	18.188	MS	–	–	–	–	–	–
<b>2076299306716922752</b>	5024211 <sup>X</sup>	1.1752	18.711	MS	–	–	–	–	–	–
<b>2076393765943855744</b>	5112994 <sup>X</sup>	1.0031	16.729	MS	–	–	–	–	–	–
<b>2076299414103588224</b>	5023913 <sup>X</sup>	18.3197	15.274	MS	–	–	–	–	–	–
2076393731584598400	5112843 <sup>X</sup>	0.1743	15.422	MS	RGB	5 600(50)	4.37(5)	42(1)	-1.4(1)	2*

## 6. The distance and age estimation

We downloaded a grid of isochrones given in the *Gaia* photometric system from the MIST project (Choi *et al.* 2016, Dotter 2016). The current version of MIST is 1.2. The MESA version 7503 was employed to calculate isochrones. We selected  $V/V_{\text{crit}}=0$ . The grid covers age in a logarithmic scale between 9.1 and 9.6 with a step of 0.01 and the iron content [Fe/H] from -0.1 to +0.1 with a step of 0.01.

For the fit, we only kept the MS, RGB and RC stars. However, in case of binary systems, the observed magnitude may include the flux contribution from all companions and not a single star, which shifts the position of a system in the CMD. To avoid biased magnitudes, we excluded outlying stars by considering their positions in the CMD as uncertain. We included magnitude uncertainties as weights in the fit, which prevented the MS targets from over-fitting. The RC and RGB targets, even though less numerous, are brighter, and hence remain significant in the fit.

The MIST synthetic isochrones are given in absolute magnitudes, and we selected no extinction. We applied a shift (m-M) in the *Gaia* G magnitude and  $B_p-R_p$  color to account for the extinction. The isochrones that fit the best are defined by two consecutive values of the age and, for each age, the same three [Fe/H] values. This solution is quite common in astrophysical modelling. The fitting shows a degeneration of solutions in which a pair of different age and [Fe/H] values compensate by providing similar quality fits. We have determined the age to be 2.54(3) Gyr and [Fe/H] to be -0.01(2). The apparent distance modulus (m-M) equals 12.20 and  $E(B_p-R_p)$  to be 0.195(10). We show the best isochrone fits in Fig. 7.

For the *Gaia* DR3 cluster members  $E(B_p-R_p)$  and interstellar extinction in the G band, the  $A_G$  form a linear relation  $A_G = 2 \cdot E(B_p-R_p)$ . Averaging the parameters from the best models we obtain  $E(B_p-R_p) = 0.194$  mag, which corresponds to  $A_G = 0.388$  mag. Subtracting  $A_G$  from (m-M) we find the true distance modulus of 11.812, which gives the distance to the cluster of 2.3 kpc.

We also derived distance from the parallaxes of the cluster members with probability membership higher than 90% and the relative parallax uncertainty smaller than 10%, which equals 2.48(18) kpc. The distance measurements from parallaxes and isochrone fits are in agreement to each other, and the age and [Fe/H] derived in our work is comparable to the results reported by Choi *et al.* (2018).

Table 5: The list of binary stars in the field that are not cluster members or no memberships derived. See caption of Table 1 for explanation. Targets with no astrometry, hence no membership established, are denoted in *italic*.

<i>Gaia</i> DR3	KIC	P <sub>orb</sub> [days]	T <sub>0</sub> [BJD]	G [mag]	T <sub>eff</sub> [K]	logg	RV [km/s]	[Fe/H]	Ref
eclipsing									
<b>2076487671098665472</b>	–	225.27602919(47) <sup>e</sup>	2 455 003.738545(5)	19.596	–	–	–	–	–
<b>2076299757701057920</b>	–	38.857349(27) <sup>e</sup>	2 454 997.2392(6)	19.489	–	–	–	–	–
<b>2076298898703420416</b>	–	0.42517143(28)	2 454 971.20746(53)	20.682	–	–	–	–	–
<b>2076297657449418880</b>	5023984 <sup>X</sup>	single-eclipse	2 455 008.4490(24)	18.400	–	–	–	–	–
<b>2076298417671214464</b>	5024527 <sup>X</sup>	30.564505(25) <sup>e</sup>	2 454 986.35489(57)	15.876	5 910(200)	4.736(22)	-75(14)	-0.68(13)	4 *
<b>2076583294245566720</b>	–	2.8083498(28)	2 454 967.2876(7)	20.461	–	–	–	–	–
2076583839713435776	5200364 <sup>X</sup>	0.206879465(16)	2 454 964.58302(7)	19.420	–	–	–	–	–
2076394590569930240	–	0.8907258(10)	2 454 965.42331(9)	20.064	–	–	–	–	–
2076394178252936704	5113146 <sup>1S/3L</sup>	18.789711(29)	2 456 216.94558(19)	19.193	–	–	–	–	–
2076390123803775104	5025294 <sup>14L</sup>	5.462678(18) <sup>e</sup>	2 455 021.8935(23)	13.246	–	–	–	–	–
<b>2076390119501429120</b>	5025349 <sup>X</sup>	50.71339(6) <sup>e</sup>	2 454 967.2679(10)	18.897	–	–	–	–	–
<b>2076298692545230848</b>	–	single-eclipse	2 455 156.9573(25)	19.816	–	–	–	–	–
active eclipsing									
<b>2076487495009192064</b>	5023833 <sup>X</sup>	1.5995032(46)	2 454 965.0930(26)	19.173	–	–	–	–	–
2076487495000121216	5023832 <sup>X</sup>	0.357122835(39)	2 454 964.69840(9)	19.523	–	–	–	–	–
<b>2076487293141296640</b>	5023901 <sup>X</sup>	318.7285(20) <sup>e</sup>	2 455 009.7943(50)	19.557	–	–	–	–	–
<b>2076487636738867328</b>	–	0.4169454(7)	2 454 965.2280(24)	19.745	–	–	–	–	–
<b>2076394006453983488</b>	–	3.0224820(6)	2 454 964.98930(15)	20.519	–	–	–	–	–
2076487254481737728	5024077 <sup>X</sup>	0.932208699(49)	2 454 965.28509(44)	13.984	16 860(230)	5.79(16)	6(5)	-4(2)	4 *
2076299276660357760	5024146 <sup>X</sup>	0.787121288(48)	2 454 964.73835(41)	15.588	5 810(200)	4.03(1)	-13(9)	-0.45(27)	4 *
2076393284907582464	5113407 <sup>X</sup>	13.826433(5) <sup>e</sup>	2 454 975.78903(29)	18.049	–	–	–	–	–
2076393044381456896	5113053 <sup>1S/4L</sup>	3.1850900(12)	2 455 466.35322(11)	20.230	–	–	–	–	–
<b>2076394659289386880</b>	5200325 <sup>X</sup>	5.3159294(28) <sup>e</sup>	2 454 969.74506(27)	17.393	5 380(200)	5.04(8)	-40(13)	-0.81(15)	4 *
contact									
2076489182934321920	5199669 <sup>X</sup>	0.758956896(42)	2 454 964.903723(46)	15.226	–	–	–	–	–
2076488285274150784	5111817 <sup>X</sup>	0.28994151(7)	2 454 964.73887(21)	19.638	–	–	–	–	–
2076487739818143360	–	0.28136943(9)	2 454 964.71482(27)	20.462	–	–	–	–	–
2076298452030939392	5024283 <sup>X</sup>	0.33846178(5)	2 454 964.58443(13)	18.044	–	–	–	–	–
<b>2076298314587607040</b>	–	0.223753315(41)	2 454 964.56924(15)	20.089	–	–	–	–	–
2076394521858125696	5112917 <sup>X</sup>	0.29314610(6)	2 454 964.66198(17)	16.878	–	–	–	–	–
<b>2076393697224860544</b>	5112791 <sup>X</sup>	0.9816957(5)	2 454 964.78683(42)	14.669	–	–	–	–	–
2076393216188094336	5113461 <sup>X</sup>	0.275128153(42)	2 454 964.73810(13)	19.632	–	–	–	–	–
2076389745856651136	5025261 <sup>15L</sup>	2.171411(7)	2 454 966.95452(29)	12.296	–	–	–	–	–
<b>2076487464939938816</b>	5023779 <sup>X</sup>	0.1963	–	17.826	–	–	–	–	–
outbursting									
2076392906942365568	–	–	–	20.427	–	–	–	–	–
<b>2076392902640277632</b>	5024812 <sup>X</sup>	–	–	16.431	–	–	–	–	–

Table 6: The list of pulsators in the field that are not cluster members or no memberships derived. See captions of Table 1 and 5 for explanation.

<i>Gaia</i> DR3	KIC	G [mag]	T <sub>eff</sub> [K]	logg	RV [km/s]	[Fe/H]	Ref
solar-like							
2076489251653787904	5199605 <sup>2L</sup>	11.496	4 250(50)	3.00(5)	0.2(1)	-0.19(3)	5 *
2076488495739440128	5111767 <sup>6L</sup>	13.641	4 524(130)	2.66(20)	-49(3)	0.20(12)	3
2076488804977149568	5111987 <sup>14L</sup>	14.949	–	–	–	–	–
<b>2076488117782408192</b>	5112211 <sup>X</sup>	14.424	–	–	–	–	–
<b>2076488014703171328</b>	5112103 <sup>X</sup>	14.804	–	–	–	–	–
<b>2076488598818838400</b>	5111863 <sup>X</sup>	14.886	–	–	–	–	–
<b>2076488873696651264</b>	5112156 <sup>X</sup>	15.403	–	–	–	–	–
<b>2076487945983698432</b>	5112169 <sup>1S,15L</sup>	10.864	6 283(11)	3.927(18)	39(4)	0.155(9)	3
2076300135658208384	5112558 <sup>10L</sup>	14.112	–	–	–	–	–
<b>2076299963859543680</b>	5024196 <sup>X</sup>	13.291	–	–	–	–	–
<b>2076299895139970816</b>	5024238 <sup>X</sup>	13.612	–	–	–	–	–
<b>2076299585902315264</b>	5024100 <sup>X</sup>	13.609	–	–	–	–	–
<b>2076299688981538944</b>	5024290 <sup>X</sup>	15.275	–	–	–	–	–
<b>2076298967427099136</b>	5024773 <sup>3L</sup>	14.325	–	–	–	–	–
<b>2076298761268662016</b>	5024804 <sup>X</sup>	15.290	–	–	–	–	–
2076299139225684096	5024043 <sup>15L</sup>	12.779	4 762(92)	2.70(11)	2.82(14)	-0.10(3)	5
<b>2076298280232974976</b>	4936972 <sup>X</sup>	13.597	–	–	–	–	–
2076296837123206912	4936825 <sup>4L</sup>	13.144	–	–	–	–	–
2076582916298933888	5199930 <sup>5L</sup>	11.893	4 260(50)	1.94(5)	0.2(3)	-0.25(9)	5 *
<b>2076582503982578944</b>	5200146 <sup>1L</sup>	11.611	4 069(144)	2.15(23)	-20(3)	-0.22(14)	3
<b>2076582297823683712</b>	5200223 <sup>X</sup>	14.140	–	–	–	–	–
<b>2076582366543185664</b>	5200359 <sup>X</sup>	13.118	–	–	–	–	–
<b>2076394693656870400</b>	5200392 <sup>X</sup>	14.772	–	–	–	–	–
<b>2076582362237411712</b>	5200367 <sup>X</sup>	13.063	–	–	–	–	–
<b>2076581919866487808</b>	5112421 <sup>X</sup>	15.505	–	–	–	–	–
<b>2076582263463928064</b>	5200143 <sup>X</sup>	15.564	–	–	–	–	–
<b>2076394418778961024</b>	5113246 <sup>X</sup>	14.720	–	–	–	–	–
<b>2076393899075590528</b>	5112672 <sup>X</sup>	16.690	–	–	–	–	–
<b>2076393594145243136</b>	5113371 <sup>X</sup>	14.452	–	–	–	–	–
<b>2076392700791972992</b>	5025162 <sup>15L</sup>	12.623	–	–	–	–	–
2076392769511450368	5025101 <sup>2L</sup>	13.003	4 404(74)	2.73(12)	-60(4)	0.10(7)	3
<b>2076389711494720640</b>	5025168 <sup>X</sup>	14.392	–	–	–	–	–
<b>2076392563352990208</b>	5025060 <sup>X</sup>	14.124	–	–	–	–	–
2076392528993243008	5025021 <sup>6L</sup>	12.842	4 675(92)	2.65(11)	38.86(46)	0.100(28)	5
δ-scuti							
<b>2076298211512787328</b>	5024570 <sup>X</sup>	16.935	7 760(60)	3.926(24)	27.1(8)	-0.57(7)	2 *
2076395896247722496	5200521 <sup>1S,15L</sup>	11.182	5 810(32)	3.535(53)	-10(6)	0.276(30)	3
γ Doradus							
<b>2076487632439073408</b>	5024090 <sup>X</sup>	19.103	–	–	–	–	–
<b>2076582602761996672</b>	5200181 <sup>X</sup>	17.216	7 150(50)	4.80(5)	-5.6(7)	-0.46(9)	2 *
<b>2076394315699722368</b>	5113250 <sup>14L</sup>	14.439	5 430(50)	3.0(1)	-51(2)	-0.65(7)	2 *
2076390192533257216	5025464 <sup>15L</sup>	13.122	7 182(30)	4.078(50)	-7(9)	-0.243(28)	3
<b>2076392627762286336</b>	5025047 <sup>X</sup>	18.250	6 930(40)	3.35(7)	45(5)	-0.40(7)	2 *
2076389642775246080	5025234 <sup>15L</sup>	13.285	–	–	–	–	–
semi-regular							
2076487808546982784	5112438 <sup>15L</sup>	10.602	3 715(69)	0.94(8)	-38.40(34)	-0.400(29)	5
2076298829988110976	5024699 <sup>15L</sup>	11.600	3 500	1	-45.9053(69)	-0.5	5
2076392632072463232	5025003 <sup>15L</sup>	8.011	–	–	–	–	–

Table 7: The list of rotational variables that are not cluster members or no memberships derived. See captions of Table 1 and 5 for explanation.

<i>Gaia</i> DR3	KIC	Period [days]	G [mag]	T <sub>eff</sub> [K]	logg	RV [km/s]	[Fe/H]	Ref
2076489006828963200	—	4.2194	20.192	—	—	—	—	—
<b>2076491656835399552</b>	5111748 <sup>X</sup>	2.2534	14.809	—	—	—	—	—
<b>2076488972469006720</b>	—	4.3523	19.439	—	—	—	—	—
<b>2076491588108521600</b>	5111658 <sup>X</sup>	11.2363	18.431	—	—	—	—	—
2076489212987407872	5199564 <sup>X</sup>	3.4612	18.809	—	—	—	—	—
<b>2076488976768870656</b>	—	4.0641	19.688	—	—	—	—	—
<b>2076491656828123904</b>	—	11.6758	19.207	—	—	—	—	—
<b>2076489109908182400</b>	—	1.8813	20.143	—	—	—	—	—
<b>2076489079855048320</b>	5111878 <sup>X</sup>	5.2625	16.775	—	—	—	—	—
2076492030485722880	5111830 <sup>X</sup>	3.1613	18.914	—	—	—	—	—
<b>2076488835030026752</b>	5112025 <sup>X</sup>	6.1208	18.934	—	—	—	—	—
<b>2076491656835403776</b>	5111760 <sup>X</sup>	6.7188	15.758	—	—	—	—	—
<b>2076491519396420864</b>	5111722 <sup>X</sup>	2.3987	19.046	—	—	—	—	—
<b>2076491618168829184</b>	5111737 <sup>X</sup>	2.1654	16.894	—	—	—	—	—
2076488873696743936	5112157 <sup>14L</sup>	27.9330	15.165	—	—	—	—	—
2076488873696744064	5112117 <sup>14L</sup>	13.6986	14.966	—	—	—	—	—
<b>2076488835038990976</b>	5112066 <sup>X</sup>	11.1315	18.715	—	—	—	—	—
2076488633178431232	5111890 <sup>14L</sup>	8.2095	13.851	—	—	—	—	—
2076488427020146176	5111932 <sup>14L</sup>	1.4345	12.215	6 556(16)	4.216(27)	-19(5)	-0.133(15)	3
<b>2076488628871828992</b>	5111870 <sup>X</sup>	5.1734	18.803	—	—	—	—	—
<b>2076488152135136256</b>	—	0.9692	20.024	—	—	—	—	—
<b>2076488113482225920</b>	5112203 <sup>X</sup>	24.0132	17.997	—	—	—	—	—
<b>2076488731950773760</b>	5112036 <sup>X</sup>	4.4587	17.976	—	—	—	—	—
2076488495732070016	5111802 <sup>X</sup>	14.2002	19.035	—	—	—	—	—
<b>2076488461379688448</b>	5111755 <sup>X</sup>	26.8169	12.863	—	—	—	—	—
<b>2076488014703180416</b>	5112144 <sup>X</sup>	26.8614	17.006	—	—	—	—	—
<b>2076488491432593024</b>	5111774 <sup>X</sup>	20.2080	17.369	—	—	—	—	—
<b>2076488427019997568</b>	5111912 <sup>X</sup>	19.7522	16.803	—	—	—	—	—
<b>2076488044756006528</b>	5112226 <sup>X</sup>	3.1371	19.372	—	—	—	—	—
<b>2076487945983706880</b>	5112224 <sup>X</sup>	7.7540	16.816	—	—	—	—	—
<b>2076487602386283520</b>	5112061 <sup>X</sup>	0.3031	16.601	—	—	—	—	—
<b>2076487872957580544</b>	5112420 <sup>X</sup>	10.1352	18.165	—	—	—	—	—
2076581644988572160	5112508 <sup>3L</sup>	0.7502	15.189	—	—	—	—	—
<b>2076487907323097600</b>	5112158 <sup>X</sup>	1.2659	18.122	—	—	—	—	—
<b>2076487705465511936</b>	5024046 <sup>X</sup>	7.2570	15.464	—	—	—	—	—
<b>2076487357561147264</b>	5023750 <sup>X</sup>	7.2731	18.786	—	—	—	—	—
2076300135658196864	5112483 <sup>14L</sup>	62.8479	11.401	—	—	—	—	—
2076487636746036736	5024079 <sup>14L</sup>	20.000	15.152	—	—	—	—	—
<b>2076487739825262976</b>	5112228 <sup>14L</sup>	21.0838	14.138	5 653(133)	4.67(0.22)	-3(6)	-0.02(13)	3
<b>2076581640685054208</b>	5112520 <sup>X</sup>	15.1677	17.561	—	—	—	—	—
<b>2076300032574913920</b>	—	0.5615	20.904	—	—	—	—	—
<b>2076487258788897792</b>	5024021 <sup>X</sup>	1.0110	19.549	—	—	—	—	—
<b>2076487293141276672</b>	5023904 <sup>X</sup>	32.5945	20.454	—	—	—	—	—
<b>2076487190069384960</b>	5023844 <sup>X</sup>	5.4594	19.614	—	—	—	—	—
<b>2076487190061988608</b>	—	0.1887	20.733	—	—	—	—	—
2076487151403028224	—	3.5949	19.612	—	—	—	—	—
<b>2076299860780304512</b>	5024541 <sup>X</sup>	7.4085	15.600	—	—	—	—	—
<b>2076299895135780224</b>	5024204 <sup>X</sup>	0.5714	19.901	—	—	—	—	—
<b>2076299551542571264</b>	5024070 <sup>X</sup>	16.2968	13.604	3 883(92)	0.73(11)	-84.49(29)	-0.500(31)	5
2076299890832483584	5024233 <sup>X</sup>	6.4642	18.150	—	—	—	—	—
2076299895139968000	5024215 <sup>14L</sup>	4.4271	13.396	6 491(42)	4.12(7)	-27(7)	0.01(40)	3
<b>2076299860776267136</b>	5024529 <sup>X</sup>	12.5097	17.884	—	—	—	—	—
2076299895135748864	5024202 <sup>11L</sup>	2.9086	17.612	—	—	—	—	—
2076299757697024128	—	6.3272	18.758	—	—	—	—	—
<b>2076299654617645056</b>	—	1.2605	19.506	—	—	—	—	—
<b>2076299684674005504</b>	5024300 <sup>X</sup>	6.6880	17.767	—	—	—	—	—
20762993453884113536	5023985 <sup>15L</sup>	6.5381	13.453	—	—	—	—	—
<b>2076299482818776704</b>	—	10.6186	19.999	—	—	—	—	—
<b>2076299753396856576</b>	5024581 <sup>X</sup>	3.9925	18.570	—	—	—	—	—
2076299207945181824	5024254 <sup>14L</sup>	34.9997	13.878	—	—	—	—	—
<b>2076299242304936192</b>	5024335 <sup>X</sup>	6.0531	15.292	—	—	—	—	—
<b>2076299139225682688</b>	5024055 <sup>X</sup>	7.1974	15.755	—	—	—	—	—
<b>2076298726908910336</b>	5024794 <sup>X</sup>	28.2478	15.957	—	—	—	—	—
<b>2076298722601233792</b>	5024811 <sup>X</sup>	2.2620	15.734	—	—	—	—	—
<b>2076298589469925632</b>	5024647 <sup>X</sup>	8.3029	15.259	—	—	—	—	—
<b>2076298795628342912</b>	5024515 <sup>X</sup>	4.7317	16.948	—	—	—	—	—
2076298310284438656	4936870 <sup>X</sup>	3.8084	17.681	—	—	—	—	—
<b>2076298314587586304</b>	4936842 <sup>X</sup>	0.7882	16.477	—	—	—	—	—
<b>2076298486386442112</b>	5024389 <sup>X</sup>	2.3891	20.433	—	—	—	—	—
2076582607061342336	5200184 <sup>13L</sup>	7.5913	15.584	—	—	—	—	—
<b>2076582534038273920</b>	5200034 <sup>X</sup>	3.8284	19.555	—	—	—	—	—

Table 8: A continuation of the list of rotational variables that are not cluster members or no memberships derived. See captions of Table 1 and 5 for explanation.

<i>Gaia</i> DR3	KIC	Period [days]	G [mag]	T <sub>eff</sub> [K]	logg	RV [km/s]	[Fe/H]	Ref
<b>2076582946355475968</b>	–	13.7111	19.060	–	–	–	–	–
<b>2076582843276554240</b>	–	7.8372	20.120	–	–	–	–	–
2076582607061335936	5200185 <sup>11L</sup>	3.7272	15.565	–	–	–	–	–
2076584118889853696	5200273 <sup>X</sup>	6.5349	16.913	4 390(60)	3.25(3)	-46(1)	-0.18(13)	1 *
<b>2076583908425657472</b>	5200352 <sup>X</sup>	6.6710	18.897	–	–	–	–	–
2076582087361668608	5199996 <sup>X</sup>	6.4674	19.317	–	–	–	–	–
<b>2076582538341833344</b>	5200036 <sup>X</sup>	21.9286	16.748	–	–	–	–	–
2076582018642530432	5112402 <sup>10L</sup>	4.8263	17.044	–	–	–	–	–
<b>2076582362237425920</b>	5200342 <sup>X</sup>	5.8353	18.743	–	–	–	–	–
<b>2076582465319431296</b>	5200038 <sup>11L</sup>	2.6316	15.154	–	–	–	–	–
<b>2076582259160998400</b>	–	4.8721	19.985	–	–	–	–	–
2076582057294883200	5112553 <sup>15L</sup>	5.2427	13.055	5 812(27)	4.595(44)	-35(4)	0.135(25)	3
<b>2076396166816178176</b>	5200463 <sup>X</sup>	0.7563	19.301	–	–	–	–	–
<b>2076581812488757632</b>	5112718 <sup>X</sup>	2.0447	18.446	–	–	–	–	–
<b>2076581679348337152</b>	5112646 <sup>X</sup>	12.5816	14.484	–	–	–	–	–
<b>2076394517550928640</b>	–	6.1322	19.448	–	–	–	–	–
2076394414469300096	5113282 <sup>X</sup>	1.4962	18.000	–	–	–	–	–
<b>2076394345749739264</b>	–	0.3484	20.151	4 503(92)	2.25(11)	-27.92(44)	-0.100(28)	5
2076394277037190656	5113103 <sup>X</sup>	5.3265	18.427	–	–	–	–	–
<b>2076394246980225280</b>	5113042 <sup>X</sup>	12.1961	16.138	–	–	–	–	–
<b>2076394075181511296</b>	5112921 <sup>X</sup>	1.040	15.961	–	–	–	–	–
<b>2076394040821761792</b>	5112865 <sup>X</sup>	8.1032	15.741	–	–	–	–	–
<b>2076394109541233536</b>	5112796 <sup>X</sup>	1.0060	17.176	–	–	–	–	–
<b>2076394105234044032</b>	5112746 <sup>X</sup>	4.5372	18.790	–	–	–	–	–
2076395071614000512	5113378 <sup>13L</sup>	24.4924	15.524	–	–	–	–	–
2076394173950795136	–	3.5243	19.318	–	–	–	–	–
<b>2076393869023082240</b>	5113011 <sup>X</sup>	10.1982	14.427	–	–	–	–	–
<b>2076393834655370240</b>	–	8.6988	19.625	–	–	–	–	–
<b>2076393456700278656</b>	–	3.7551	20.610	–	–	–	–	–
<b>2076393903374713856</b>	5112711 <sup>X</sup>	8.4417	17.731	–	–	–	–	–
2076393491065999360	5113306 <sup>X</sup>	1.9503	18.317	–	–	–	–	–
2076393353627026944	5113228 <sup>1L</sup>	4.9268	12.332	4 030(92)	1.19(11)	-6.277(22)	-0.100(28)	5
<b>2076393795993621376</b>	5113037 <sup>X</sup>	2.6187	20.041	–	–	–	–	–
2076393658557409792	5024787 <sup>14L</sup>	12.7227	17.924	–	–	–	–	–
2076392765201345280	5025129 <sup>X</sup>	9.5598	17.830	–	–	–	–	–
<b>2076392872590618112</b>	–	7.2291	19.511	–	–	–	–	–
<b>2076393250540210432</b>	5113521 <sup>X</sup>	0.9759	18.448	–	–	–	–	–
2076393211878004096	5113452 <sup>X</sup>	0.7334	18.605	–	–	–	–	–
<b>2076393113108873344</b>	5113418 <sup>X</sup>	12.8024	17.779	–	–	–	–	–
<b>2076393108798746752</b>	5113384 <sup>X</sup>	1.3900	17.050	–	–	–	–	–
<b>2076392971359814528</b>	5113140 <sup>X</sup>	7.9415	18.691	–	–	–	–	–
<b>2076392838230901632</b>	5024960 <sup>X</sup>	9.2894	15.874	–	–	–	–	–
<b>2076392872582614144</b>	–	17.6075	18.606	–	–	–	–	–
<b>2076390192531117440</b>	5025475 <sup>X</sup>	5.4480	17.747	–	–	–	–	–
<b>2076390055084332672</b>	5025381 <sup>X</sup>	5.8275	19.118	–	–	–	–	–
2076389604105250560	5025159 <sup>X</sup>	3.3906	19.053	–	–	–	–	–
<b>2076390020724772736</b>	5025605 <sup>X</sup>	12.1848	18.306	–	–	–	–	–
<b>2076389711494726272</b>	5025195 <sup>X</sup>	13.1484	18.311	–	–	–	–	–
<b>2076390050781929472</b>	5025372 <sup>X</sup>	0.9905	18.329	–	–	–	–	–
<b>2076392559042768896</b>	5025092 <sup>X</sup>	4.4708	19.278	–	–	–	–	–
<b>2076488942409044864</b>	–	1.4495	–	–	–	–	–	–
<b>2076581988577868032</b>	–	3.9648	21.031	–	–	–	–	–
<b>2076488049065148288</b>	5112292 <sup>X</sup>	1.9006	16.004	–	–	–	–	–
<b>2076487739818146048</b>	–	3.8497	21.192	–	–	–	–	–
<b>2076487224431395712</b>	–	2.2195	20.442	–	–	–	–	–
<b>2076581919858187136</b>	–	7.4127	20.923	–	–	–	–	–
<b>2076581748057139456</b>	–	17.6544	21.159	–	–	–	–	–
<b>2076487464947285248</b>	5023707 <sup>X</sup>	0.9582	15.199	–	–	–	–	–
<b>2076392941302191616</b>	–	0.6279	20.924	–	–	–	–	–
<b>2076394620627810432</b>	5200435 <sup>X</sup>	0.6398	18.505	–	–	–	–	–
<b>2076394384411491712</b>	5113161 <sup>X</sup>	2.2842	19.132	–	–	–	–	–
2076491588108524160	5111658 <sup>X</sup>	1.3542	16.277	4 470(60)	4.572(57)	-89(1)	-0.76(6)	2 *
<b>2076491588108524160</b>	–	1.9159	17.492	–	–	–	–	–
<b>2076298310287835776</b>	4936866 <sup>X</sup>	1.3921	18.014	–	–	–	–	–
<b>2076390123803764352</b>	–	3.9365	15.646	–	–	–	–	–

Table 9: The list of unclassified variables that are not identified as cluster members in our analysis. See captions of Table 1 and 5 for explanation.

<i>Gaia</i> DR3	KIC	Period [days]	G [mag]
<b>2076489011128317824</b>	5111916 <sup>X</sup>	0.2954	19.854
<b>2076488495732906496</b>	5111771 <sup>X</sup>	0.6336	20.106
<b>2076487533659553024</b>	5112097 <sup>X</sup>	0.2629	19.411
<b>2076299998215027968</b>	–	0.7388	20.198
<b>2076487224421838336</b>	–	0.5368	19.785
<b>2076299826420547200</b>	5024510 <sup>X</sup>	3.1140	14.827
<b>2076299895135783168</b>	–	0.4290	20.698
<b>2076298447723494016</b>	5024319 <sup>X</sup>	0.3007	19.934
<b>2076298791320709120</b>	5024566 <sup>X</sup>	0.7352	18.553
<b>2076394517548400896</b>	5112901 <sup>X</sup>	0.6911	19.291
<b>2076394384411456000</b>	5113175 <sup>X</sup>	0.1723	18.885
<b>2076393314960052480</b>	–	0.4764	20.839
<b>2076393108798736384</b>	5025311 <sup>X</sup>	1.9564	15.472
<b>2076392528993235968</b>	5024986 <sup>X</sup>	0.3169	16.960
<b>2076581984282789632</b>	5112326 <sup>X</sup>	0.1085	17.258
<b>2076487838597567104</b>	5112332 <sup>X</sup>	6.4325	18.557
<b>2076393869023083776</b>	–	2.9235	18.391
<b>2076390123803775104</b>	–	3.3921	18.469

Table 10: A list of equatorial coordinates that are associated with the superstamp pixels showing signal in their amplitude spectra. The only coordinates not marked in bold were associated with a variable star NGC 6819 SHLP 25645 and reported by Street *et al.* (2002).

$\alpha_{2000}$ [hh mm ss.ss]	$\delta_{2000}$ [dd mm ss.s]	Period [days]	Type
<b>19 41 20.77</b>	<b>+40 17 18.77</b>	0.8824	eclipsing
<b>19 40 57.78</b>	<b>+40 10 11.87</b>	0.5085	active eclipsing
19 40 57.99	+40 19 00.30	0.2734	contact
<b>19 41 0.81</b>	<b>+40 18 20.35</b>	0.2342	contact
<b>19 41 10.24</b>	<b>+40 10 35.73</b>	0.2080	contact
<b>19 41 23.73</b>	<b>+40 18 54.4</b>	65.3493	outbursting
<b>19 41 28.59</b>	<b>+40 11 31.17</b>	29.6949	outbursting
<b>19 41 29.61</b>	<b>+40 11 19.35</b>	45.4381	outbursting
<b>19 40 48.17</b>	<b>+40 13 12.24</b>	0.4093	rotating
<b>19 41 13.06</b>	<b>+40 10 37.26</b>	0.6044	rotating
<b>19 40 53.45</b>	<b>+40 08 43.40</b>	0.3261	rotating
<b>19 40 57.85</b>	<b>+40 07 31.53</b>	0.7897	rotating
<b>19 41 25.84</b>	<b>+40 08 21.47</b>	2.6166	rotating
<b>19 41 26.11</b>	<b>+40 06 58.64</b>	1.7384	rotating
<b>19 41 15.77</b>	<b>+40 05 52.16</b>	8.1636	rotating
<b>19 41 23.23</b>	<b>+40 18 31.1</b>	2.2959	rotating
<b>19 41 27.12</b>	<b>+40 16 25.39</b>	3.7529	rotating
<b>19 41 16.70</b>	<b>+40 15 34.46</b>	2.0277	rotating
<b>19 41 41.79</b>	<b>+40 16 43.86</b>	15.2913	rotating
<b>19 41 28.35</b>	<b>+40 13 1.84</b>	41.1247	rotating
<b>19 41 47.97</b>	<b>+40 12 21.28</b>	0.2771	rotating
<b>19 41 37.49</b>	<b>+40 09 3.74</b>	52.5409	rotating
<b>19 41 50.89</b>	<b>+40 10 28.79</b>	0.9870	rotating
<b>19 41 6.38</b>	<b>+40 14 53.84</b>	0.3660	unclassified



We also plotted isochrones in the  $T_{\text{eff}}$  and  $\log g$  plane (HRD) shown in Fig. 8. We used the isochrones for the age and  $[\text{Fe}/\text{H}]$ , which we derived from the isochrone fitting in the CMD. We overplotted the isochrones with our variable stars from Tables 1-3, for which  $T_{\text{eff}}$  and  $\log g$  are listed. The column 'HRD' in Tables 1-4 describes the location of a given star in the HRD. If the location agrees with the one in the CMD, we can expect the spectroscopic fit is likely correct. We obtained an agreement in all but two cases. One of the exceptions is a rotational variable KIC 5113295. In both cases, as the CMD shows, the gravity of MS stars is around 4.5.

## 7. Summary

We presented a search for variable stars in the *Kepler* superstamp data of NGC 6819. Individual pixels were searched, by means of a Fourier amplitude spectrum, and contiguous apertures for each object that shows a significant flux variation were defined. The coordinates of these optimal apertures were matched with optical counterparts using the Pan-STARRS survey. In total, we detected 385 variable stars. We searched the literature for variable stars reported prior to our work, and we found that 27 variable stars were reported by Street *et al.* (2002), eight by Street *et al.* (2005), one from the All Sky Automated Survey (ASAS) catalogue by Pigulski *et al.* (2009), 75 from VSX by Watson *et al.* (2006), 21 from General Catalogue of Variable Stars (GCVS) and from New Catalogue of Variable Stars (NSV) by Samus (2017). We found 306 stars having KIC designations, out of which 226 stars do not have any data delivered to the MAST. For 270 stars, their variable nature was unknown prior to our analysis. These stars are marked in bold in Tables 1-10.

Using *Gaia* DR3 astrometry, we calculated the membership probabilities for all variable stars in our sample by applying Bayesian Gaussian mixture models. We considered a star to be a cluster member if its membership probability is higher than 50%. In total, we found 128 cluster member variables, including 17 binaries, 24 pulsators, 82 rotationally and five unclassified. The locations of these cluster variable stars in the CMD diagram indicate their evolutionary status. In the CMD, a majority of our variable stars are located on the MS, while solar-like pulsators are mostly split into the RGB and RC, semi-regular variables are located on the AGB, and five in the BS region.

In the case of selected binary systems, we estimated mid-times of eclipses or minima of a continuous flux variation and derived ephemerides. We calculated the O-C diagrams and checked for any orbital period variation. Four binary systems show significant period variation, however its nature is not confirmed. The solar-like as well as  $\delta$  Scuti and  $\gamma$  Doradus pulsators have been a subject of a detailed analysis of its pulsation content, and the results will be published by Themessl *et al.* (in prep.) and Guzik *et al.* (2023), respectively.

We used publicly available spectra of 42 variable stars. In addition, we analyzed spectra of eight stars collected with the 2.51 m NOT and spectra of five stars were taken with the 3.5 m APO telescopes. For the latter spectra, we quote a minimum uncertainty of 200 K due to the low S/N. Spectra of 21 stars were fitted with the XTGRID, while

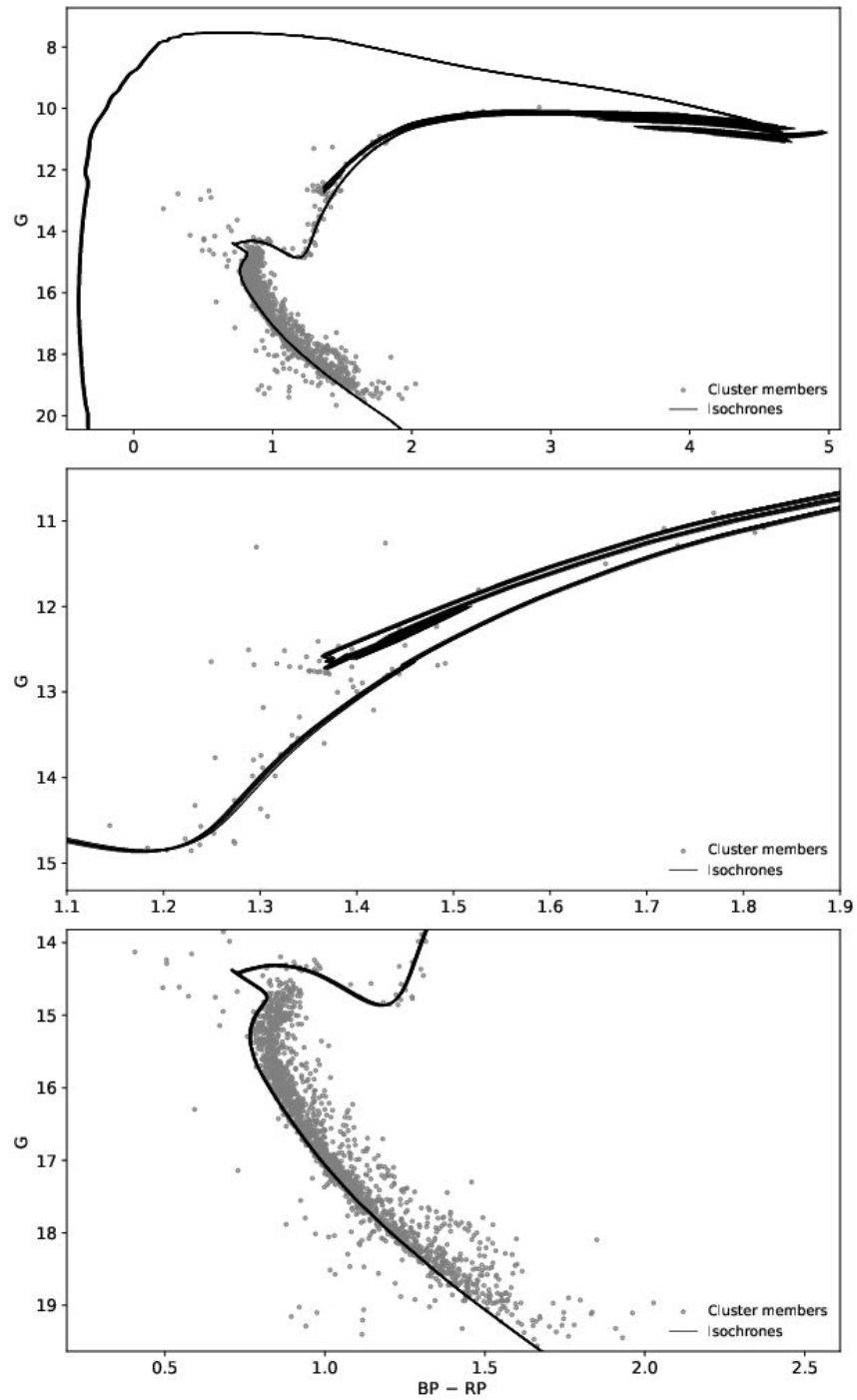


Figure 7: Color-magnitude diagram of NGC 6819, showing the best MIST isochrone fits. The top panel shows the overall diagram, while the middle panel shows the red clump region and the bottom panel shows the main-sequence region.

for the remainder of the sample, we adopted the fit values from the surveys. We derived  $T_{\text{eff}}$ ,  $\log g$ ,  $[\text{Fe}/\text{H}]$  and RVs. Thanks to our spectral analysis we were able to recover consistent stellar parameters from very diverse spectroscopic data. This consistency is reflected by the similar distribution of stars in the CMD and HRD.

We used MIST isochrones to fit the positions of the cluster members in the CMD. Our variable star population was also included in the fit. The best solution was achieved for six isochrones giving  $[\text{Fe}/\text{H}]$  of  $-0.01(2)$  and the age of  $2.54(3)$  Gyr. The age estimate agrees with the value reported by Choi *et al.* (2018). The average distance estimate from the distance modulus is 2.3 kpc, which is in agreement with our independent estimate of  $2.48(18)$  kpc derived from the *Gaia* astrometry of a selected sample of the cluster members.

## Acknowledgement

Financial support from the National Science Centre under projects No. UMO-2017/26/E/ST9/00703 and UMO-2017/25/B/ST9/02218 is acknowledged. PN acknowledges support from the Grant Agency of the Czech Republic (GAČR 22-34467S). The Astronomical Institute in Ondřejov is supported by the project RVO:67985815. This paper includes data collected by the Kepler mission and obtained from the MAST data archive at the Space Telescope Science Institute (STScI). Funding for the Kepler mission is provided by the NASA Science Mission Directorate. STScI is operated by the Association of Universities for Research in Astronomy, Inc., under NASA contract NAS 5-26555. This work has made use of data from the European Space Agency (ESA) mission. *Gaia* (<https://www.cosmos.esa.int/gaia>), processed by the *Gaia* Data Processing and Analysis Consortium (<https://www.cosmos.esa.int/web/gaia/dpac/consortium>). Funding for the DPAC has been provided by national institutions, in particular, the institutions participating in the *Gaia* Multi-lateral Agreement. This research has made use of the NASA/IPAC Extragalactic Database (NED), which is operated by the Jet Propulsion Laboratory, California Institute of Technology, under contract with the National Aeronautics and Space Administration. Based on observations obtained with the Apache Point Observatory 3.5-meter telescope, which is owned and operated by the Astrophysical Research Consortium (<https://www.apo.nmsu.edu>). This research has used the services of [www.Astroserver.org](http://www.Astroserver.org) under reference YIE7AQ and ZLNV9K.

## References

- Ahn C. P. et al., 2014, ApJ, 211, 17  
Ak T., Bostanci Z. F., Yontan T., Bilir S., Guver T., Ak S., Urgup H., Paun-zen E., 2016, Ap&SS, 361, 126  
Anthony-Twarog B. J., Deliyannis C. P., Twarog B. A., 2014, AJ, 148, 51  
Auner G., 1974, A&AS, 13, 143  
Balona L. A., et al., 2013, MNRAS, 430, 3472

Baran A., 2013, *AcA*, 63, 203

Barkhatova K.A., Vasilevsky A.E., 1967, *Peremennye Zvezdy*, 16, 191

Barnard E. E., 1931, *Publications of the Yerkes Observatory*, 6, 1

Basu S. et al., 2011, *ApJ*, 729, L10

Bohlin, R. C., Mészáros, S., Fleming, S. W., et al., 2017, *AJ*, 153, 234

Bragaglia A., et al., 2001, *AJ*, 121, 327

Burkhead M. S., 1971, *AJ*, 76, 251

Cantat-Gaudin T., et al, 2018, *AAP*, 618, A93

Chambers K. C. et al., 2016, *arXiv*, 1612, 05560

Choi J., Dotter A., Conroy C., Cantiello M., Paxton B., Johnson B. D., 2016, *ApJ*, 823, 102

Choi J., et al., 2018, *ApJ*, 863, 65

Colman I. L. et al., 2022, *ApJS*, 258, 39

Dotter A., 2016, *ApJS*, 222, 8

Fabricant D. et al., 2005, *PASP*, 117, 1411

Ferguson T. S., 1973, *The Annals of Statistics*, 1, 209

Flewelling H. A. et al., 2020, *ApJ*, 251, 7

Friel, et al., 1989, *PASP*, 101, 1105-1112

Gaia Collaboration et al., 2022, *A&A*, accepted

Gao X.-H., Xu S.-K., Chen L., 2015, *Research in Astronomy and Astrophysics*, 15, 2193

Gosnell N. M., et al., 2012, *APJ*, 745, 57

Guzik J., et al., 2023, *ApJ*, accepted

Hole K. T., Geller A. M., Mathieu R. D., Platais I., Meibom S., Latham D. W., 2009, *AJ*, 138, 159

Hoskin M., 2005, *Journal for the History of Astronomy*, 36, 373-406

Kalirai J. S., et al., 2001, *AJ*, 122, 266

Kaluzny J., Shara M. M., 1988, *AJ*, 95, 785

Kamann S., Bastian N. J., Gieles M., Balbinot E., Hénault-Brunet V., 2018, *MNRAS*, 483, 2197

Kinemuchi K., et al., 2012, *Publications of the Astronomical Society of the Pacific*, 124, 963

King I. R., 1964, *Royal Greenwich Observatory Bulletins*, 82, 106

Kryachko T.V., 2001, *Information Bulletin on Variable Stars*, 5058, 1

Kwee K., van Woerden H., 1956, *Bulletin of the Astronomical Institutes of the Netherlands*, 12, 327

Lee-Brown D. B., Anthony-Twarog B. J., Deliyannis C. P., Rich E., Twarog B. A., 2015, *AJ*, 149, 121

Lindoff U., 1972, *A&AS*, 7, 497

Lindoff U., 1971, *Information Bulletin on Variable Stars*, 606, 01

Majewski S. R. et al., 2017, *AJ*, 154, 94

Manteiga M., et al., 1989, *AAP*, 210, 66-77

Németh, P., Kawka, A., Vennes, S., 2012, MNRAS, 427, 2180

Pedregosa F., et al., 2011, Journal of Machine Learning Research, 12, 2825

Pigulski A., et al., 2009, AcA, 59, 33

Platais I., Gosnell N. M., Meibom S., Kozhurina-Platais V., Bellini A., Veillet C., Burkhead M. S., 2013, AJ, 146, 43

Purgathofer A., 1966, Mitteilungen der Universitaets-Sternwarte Wien, 13, 7

Rosvick J. M., Vandenberg D. A., 1998, AJ, 115, 1516

Salaris M., Weiss A., Percival S. M., 2004, AAP, 414, 163

Sampedro L., et al., 2017, MNRAS, 470, 3937

Samus N.N., et al., 2017, Astronomy Reports, 61, 80-88

Sanders W. L., 1972, A&A, 19, 155

Samus N.N., et al., 2017, Astronomy Reports, 61, 80-88

Sanders W. L., 1972, A&A, 19, 155

Sanjayan S., et al., 2022a, AcA, 72, 77

Sanjayan S., et al., 2022b, MNRAS, 509, 763-777

Stello D., et al., 2010, Astronomische Nachrichten, 331, 985

Stello D., et al., 2011, ApJ, 739, 13

Street R. A., et al., 2002, MNRAS, 330, 737

Street R. A., et al., 2003, MNRAS, 340, 1287

Street R. A., et al., 2005, MNRAS, 358, 795

Talamantes A., Sandquist E. L., Clem J. L., Robb R. M., Balam D. D., Shetrone M., 2010, AJ, 140, 1268

Themessl N., et al., in prep., -, -, -

Tody D., 1986, SPIE Conference Series, 627, 733

Tody D., 1993, ASP Conference Series, 52, 173

Watson C.L., Henden A.A. and Price A., Society for Astronomical Sciences Annual Symposium, 2006, 25, 47

Zhang Bo., et al., 2015, Research in Astronomy and Astrophysics, 15, 1197

Zhao G. et al., 2012, RA&A, 12, 7

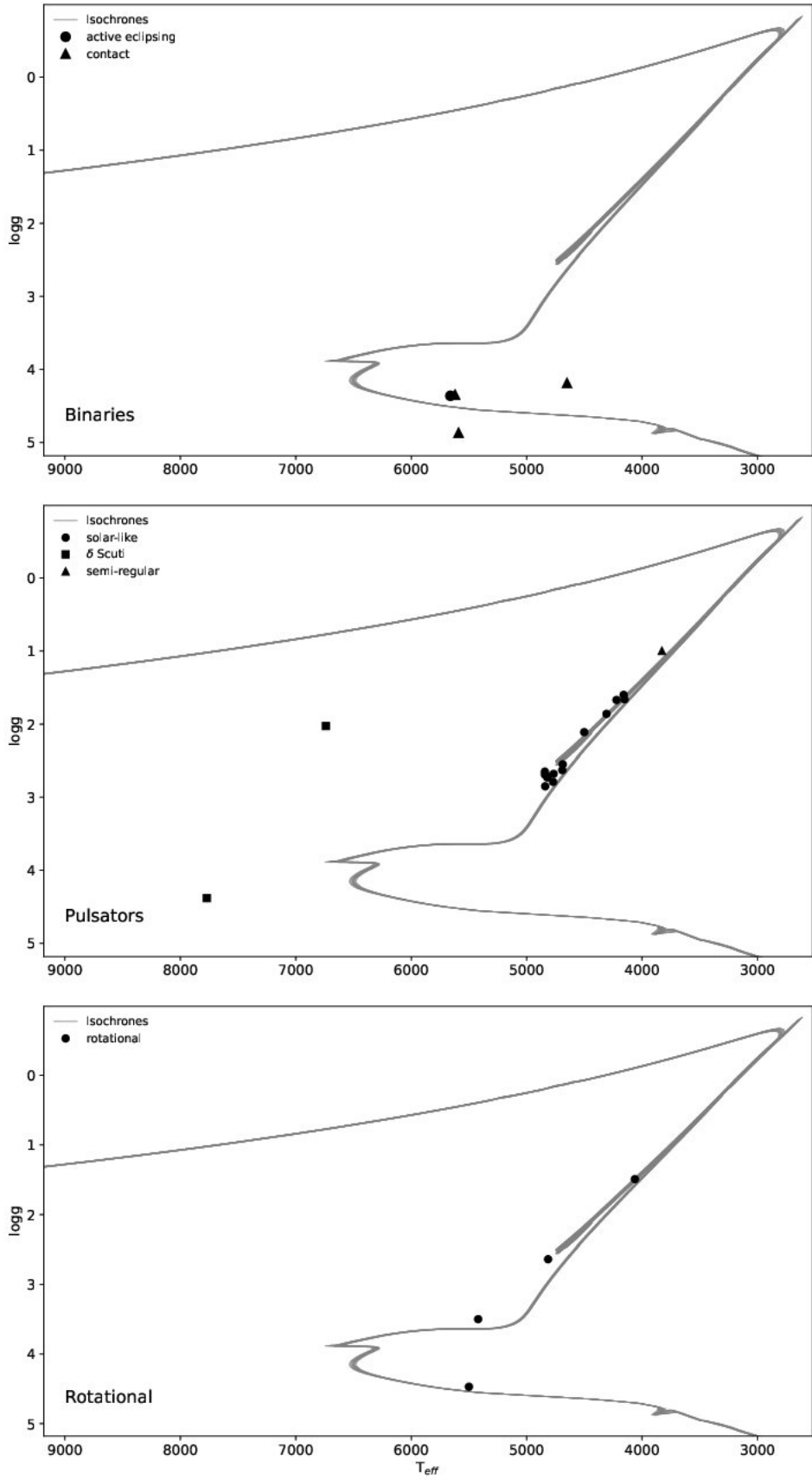


Figure 8:  $T_{\text{eff}}\text{-}\log g$  diagram showing the cluster members with atmospheric parameters derived in this work. The top, middle, and bottom panels show binary, pulsating, and rotating stars, respectively. The isochrones represent the best MIST fits in the CMD plotted in  $T_{\text{eff}}$  and  $\log g$  space.